



LJMU Research Online

Khan, I, Hussein, S, Houacine, C, Khan Sadozai, S, Islam, Y, Bnyan, R, Elhissi, A and Yousaf, S

Fabrication, characterization and optimization of nanostructured lipid carrier formulations using Beclomethasone dipropionate for pulmonary drug delivery via medical nebulizers

<http://researchonline.ljmu.ac.uk/id/eprint/14524/>

Article

Citation (please note it is advisable to refer to the publisher's version if you intend to cite from this work)

Khan, I, Hussein, S, Houacine, C, Khan Sadozai, S, Islam, Y, Bnyan, R, Elhissi, A and Yousaf, S (2021) Fabrication, characterization and optimization of nanostructured lipid carrier formulations using Beclomethasone dipropionate for pulmonary drug delivery via medical

LJMU has developed **LJMU Research Online** for users to access the research output of the University more effectively. Copyright © and Moral Rights for the papers on this site are retained by the individual authors and/or other copyright owners. Users may download and/or print one copy of any article(s) in LJMU Research Online to facilitate their private study or for non-commercial research. You may not engage in further distribution of the material or use it for any profit-making activities or any commercial gain.

The version presented here may differ from the published version or from the version of the record. Please see the repository URL above for details on accessing the published version and note that access may require a subscription.

For more information please contact researchonline@ljmu.ac.uk

<http://researchonline.ljmu.ac.uk/>



LJMU Research Online

Khan, I, Hussein, S, Houacine, C, Khan Sadozai, S, Islam, Y, Bnyan, R, Elhissi, A and Yousaf, S

Fabrication, characterization and optimization of nanostructured lipid carrier formulations using Beclomethasone dipropionate for pulmonary drug delivery via medical nebulizers

<http://researchonline.ljmu.ac.uk/id/eprint/14524/>

Article

Citation (please note it is advisable to refer to the publisher's version if you intend to cite from this work)

Khan, I, Hussein, S, Houacine, C, Khan Sadozai, S, Islam, Y, Bnyan, R, Elhissi, A and Yousaf, S (2021) Fabrication, characterization and optimization of nanostructured lipid carrier formulations using Beclomethasone dipropionate for pulmonary drug delivery via medical

LJMU has developed **LJMU Research Online** for users to access the research output of the University more effectively. Copyright © and Moral Rights for the papers on this site are retained by the individual authors and/or other copyright owners. Users may download and/or print one copy of any article(s) in LJMU Research Online to facilitate their private study or for non-commercial research. You may not engage in further distribution of the material or use it for any profit-making activities or any commercial gain.

The version presented here may differ from the published version or from the version of the record. Please see the repository URL above for details on accessing the published version and note that access may require a subscription.

For more information please contact researchonline@ljmu.ac.uk

<http://researchonline.ljmu.ac.uk/>

Fabrication, Characterization and Optimization of Nanostructured Lipid Carrier Formulations using Beclomethasone Dipropionate for Pulmonary Drug Delivery via Medical Nebulizers

Iftikhar Khan^{1*}, Sozan Hussein¹, Chahinez Houacine², Sajid Khan Sadozai³, Yamir Islam¹, Ruba Bnyan¹, Abdelbary Elhissi⁴, Sakib Yousaf³

¹School of Pharmacy and Biomolecular Sciences, Liverpool John Moores University, Liverpool L3 3AF, United Kingdom

²School of Pharmacy and Biomedical Sciences, University of Central Lancashire, Preston PR1 2HE, United Kingdom

³Department of Pharmacy, Kohat University of Science and Technology, Kohat, Pakistan

⁴Pharmaceutical Sciences Section, College of Pharmacy, Qatar University, P.O. Box 2713, Doha, Qatar.

Corresponding authors:

*Iftikhar Khan

School of Pharmacy and Biomolecular Sciences,
Liverpool John Moores University,
Liverpool L3 3AF,
United Kingdom

T: (+44) 151 231 2736

E-mail: I.Khan@ljmu.ac.uk, iftikharkhans@yahoo.com

Abstract

Aerosolization is a non-invasive approach in drug delivery for localized and systemic effect. Nanostructured lipid carriers (NLCs) are new generation versatile carriers, which offer protection from degradation and enhance bioavailability of poorly water soluble drugs. The aim of this study was to develop and optimize NLC formulations in combination with optimized airflow rates (i.e. 60 and 15 L/min) and choice of medical nebulizers including Air jet, Vibrating mesh and Ultrasonic nebulizer for superior aerosolization performance, assessed via a next generation impactor (NGI). Novel composition and combination of NLC formulations (F1 – F15) were prepared via ultrasonication method, employing five solid lipids (glycerol trimyristate (GTM), glycerol trilaurate (GTL), cetyl palmitate (CP), glycerol monostearate (GMS) and stearic acid (SA)); and three liquid lipids (glyceryl tributyrate (GTB), propylene glycol dicaprylate/dicaprate (PGD) and isopropyl palmitate (IPP)) in 1:3 w/w ratios (i.e. combination of one solid and one liquid lipid), with Beclomethasone dipropionate (BDP) incorporated as the model drug. Out of fifteen BDP-NLC formulations, the physicochemical properties of formulations F7, F8 and F10 exhibited desirable stability (one week at 25 °C), with associated particle size of ~241 nm, and >91% of drug entrapment. Post aerosolization, F10 was observed to deposit notably smaller sized particles (from 198 to 136 nm, 283 to 135 nm and 239 to 157 nm for Air jet, Vibrating mesh and Ultrasonic nebulizers, respectively) in all stages (i.e. from stage 1 to 8) of the NGI, when compared to F7 and F8 formulations. Six week stability studies conducted at 4, 25 and 45 °C, demonstrated F10 formulation stability in terms of particle size, irrespective of temperature conditions. Nebulizer performance study using the NGI for F10 identified the Air jet to be the most efficient nebulizer, depositing lower concentrations of BDP in the earlier stages (1 – 3) and higher (circa 82 and 85%) in the lateral stages (4 – 8) using 60 and 15 L/min airflow rates, when compared to the Vibrating mesh and Ultrasonic nebulizers. Moreover, at both airflow rates, the Air jet nebulizer elicited a longer nebulization time of ~42 min, facilitating aerosol inhalation for prophylaxis of asthma with normal tidal breathing. Based on characterization and nebulizer performance employing both 60 and 15 L/min airflow rates, the Air jet nebulizer offered enhanced performance, exhibiting a higher fine particle dose (FPD) (90 and 69 µg), fine particle fraction (FPF) (70 and 54%), respirable fraction (RF) (92 and 69%), and lower mass median aerodynamic diameter (MMAD) (1.15 and 1.62 µm); in addition to demonstrating higher drug deposition in the lateral parts of the NGI, when compared to its counterpart nebulizers. The F10 formulation used with the Air jet nebulizer was identified as being the most suitable combination for delivery of BDP-NLC formulations.

Keywords: Nanostructured lipid carriers; Nebulizers; Aerosolization; Pulmonary system; Beclomethasone dipropionate; Next generation impactor; Drug delivery

1. Introduction

Increased interest in the usage of the pulmonary system for not only localised but systemic delivery has been observed in recent years (Pindiprolu et al., 2020). This is particularly so for water soluble drugs which exhibit low bioavailability when administered through alternative routes (Heinemann et al., 2001). The pulmonary system offers a highly vascularised large surface area of circa 100 m², in combination with a thin alveolar epithelium, facilitating rapid absorption (Khan et al., 2016, Malamatarı et al., 2020). This is in addition to low enzymatic activity (both intra and extracellular) in the system, which negates potential drug degradation. Following pulmonary administration, a relatively high extent of absorption can be achieved for drugs with associated low absorption rates. For localized treatment of pulmonary diseases states, direct formulation deposition onto the lung epithelium facilitates rapid onset of action, with lower doses required.

In the preceding decades, nano-carriers have gained popularity for the delivery of therapeutically active compounds into pulmonary system, in order to fulfil several requirements including; shielding drug degradation, drug loading ability, sustained release, biodegradation and biocompatibility; as well as formulation stability during nebulization using various nebulizers. Various lipid-based formulations fulfil these requirements and have successfully delivered APIs (active pharmaceutical ingredients) into the pulmonary system, these include: liposomes and proliposomes (Khan et al., 2018, Elhissi, 2017, Elhissi et al., 2011, Gala et al., 2015, Bnyan et al., 2020), transfersomes and protransfersomes (Bnyan et al., 2019, Khan et al., 2020a, Subramanian et al., 2016, Bnyan et al., 2018), niosomes and proniosomes (Najlah et al., 2015, Muzzalupo and Mazzotta, 2019), ethosomes and nano-emulsions (Nasri et al., 2020, Pavoni et al., 2020, Nesamony et al., 2014), polymeric nanoparticles (Jarai et al., 2020, d'Angelo et al., 2015) and solid lipid nanoparticles (Liu et al., 2008, Esmaili et al., 2016). Lipid nanoparticles are a popular research avenue for the delivery of hydrophobic drugs. Solid lipid nanoparticles (SLNs) are first generation of lipid nanoparticles, where nanoparticles of a solid lipid matrix are dispersed in an aqueous dispersion, which is stabilized by the addition of one or more emulsifying agents. SLNs offer various advantages, including: biocompatibility, economical scale-up process, and protection of moisture sensitive and photosensitive compounds (Mehnert and Mäder, 2001). SLNs are however also associated with limited drug loading ability, particle growth and stability issues resulting in drug expulsion. This has driven the development of second generation lipid nanoparticles, referred to as nanostructured lipid carriers (NLCs). NLCs are essentially based on a mixture comprised of solid and liquid lipid. The incorporation of oil in the solid lipid matrix of lipid nanoparticles

circumvents the crystallization process, constructing imperfections in the NLC structure, encapsulating higher concentrations of drug, as well increasing nanoparticle stability. Additionally, unlike SLNs, NLCs do not suffer from expulsion of poorly water soluble APIs from the matrix of nanoparticles (Haider et al., 2020, Subramaniam et al., 2020).

Nebulizers are used to deliver the particulate based drug delivery systems into the pulmonary system. Medical nebulizers are commercially available in three types, these are; Air jet, Vibrating mesh and Ultrasonic. All have been employed extensively for lipid-based formulations in the treatment of pulmonary diseases. These nebulizers generate aerosols from formulation suspension/solution for their deposition into the respiratory tract. Air jet nebulizer use compressed gas, passing through venture nozzle, where formulation is drawn from the nebulizer reservoir making a fine filament which collapse into aerosol droplets. Ultrasonic nebulizer using piezoelectric crystal (produces high frequency vibration) to generate a fountain of formulation-air interface, resulting in the formation of aerosol droplets. Vibrating mesh nebulizer employing perforated plate through which formulation is extruded to generate aerosols (Dhand, 2002).

One of the traditional method and considered as “the golden standard” method is the impactor recommended by United State Pharmacopeia and European Pharmacopeia for inhalation, where it yield mass fraction of the drug dose (quantified by analysis) in the aerodynamic size classes (i.e. stages) that are pertinent to the particle size deposition in the human respiratory tract. Particles deposition performance is relevant to the combine effect of inertial impaction, sedimentation and Brownian diffusion giving representative simulation of deposition in the lungs (Khan et al., 2013, Zhang et al., 2014). In this regard, next generation impactor (NGI) is the commercially available model measuring the aerodynamic diameter of aerosol particles to meet the requirement of European Pharmacopeia and United State Pharmacopeia. The NGI was originally calibrated for the airflow rate of 30 to 100 L/min, but a separate calibration was carried out by European Pharmaceutical Aerosol Group (EPAG) employing 15 L/min in order to confirm NGI suitability for nebulizers (Copley, 2008, Marple et al., 2003). To meet the requirements, an airflow rate of 15 L/min was employed using medical nebulizers. Furthermore, for comparison and investigation purposes, four time higher airflow rate i.e. 60 L/min was also operated to identify differences in nebulization performance (BDP deposition in NGI stages, mass output, output rate, FPD, FPF, RF, MMAD and GSD) using three different medical nebulizers, when compared to the airflow rate of 15 L/min. However, it is noteworthy that the high and low airflow rates do not affect the generation of aerosol from the BDP-NLC suspension formulations in the nebulizers but may change the size and droplets, as well as their deposition and travelling in various stages of NGI post aerosol generation.

In this study, novel BDP-NLC formulations employing the corticosteroid beclomethasone dipropionate (BDP) were developed, optimized and characterized for their deposition in the NGI. The impact of formulation contained a unique composition and combination of solid lipid with liquid lipid and surfactant type was explored followed by investigating the following parameters, namely: particle size, size distribution, Zeta potential and drug entrapment. Furthermore, NLC formulations were tested for the first time on a variety of nebulizer types based on different operation mechanism including Air jet, Vibrating mesh and Ultrasonic nebulizer. Additionally, this is the first study where their nebulization performance using NGI employing two airflow rates (60 and 15 L/min) are examined in addition to stability studies (4, 25 and 45 °C).

2. Materials and methods

2.1. Materials

Beclomethasone dipropionate (BDP), Tween 80, Isopropyl palmitate were purchased from Sigma Aldrich, UK. Propylene glycol dicaprylate/dicaprate (Miglyol 840), glycerol trimyristate (Trimyristin) were a generous gift from Oleo chemicals, UK. Stearic acid, Glycerol trilaurate (Trilaurin), Sodium taurocholate hydrate, Glycerol monostearate, Cetyl palmitate (Palmityl palmitate) were acquired from Alfa aesar, UK. Analytical grade methanol, glycerol tributyrinate (Tributyryn) and Millipore filter (3 kDa) were obtained from Fisher Scientific, UK. Soya phosphatidylcholine (Lipoid; S – 100) was purchased from Lipoid, Switzerland. Carbon coated copper grid (400 mesh) were bought from TAAB laboratories equipment Ltd., UK.

2.2. Preparation and optimization of Nanostructured Lipid Carriers (NLCs)

Five different types of solid lipid along with three different types of liquid lipids were used in a ratio of 1:3 (w/w) to prepare 15 different BDP-NLC formulations via ultrasonication method. Solid lipid employed included, two triglycerides (glycerol trimyristate (GTM) and glycerol trilaurate (GTL)), one palmitate ester (cetyl palmitate (CP)), one monoglyceride (glycerol monostearate (GMS) and one long-chain fatty acid (stearic acid (SA)); and three liquid lipids, one triglyceride (glyceryl tributyrinate (GTB)), one diglyceride (propylene glycol dicaprylate/dicaprate (PGD)) and one fatty acid ester (isopropyl palmitate (IPP)). Each formulation was prepared using three phases i.e., lipid phase, aqueous phase and drug phase (Table 1).

A hot lipid phase was prepared by employing one of solid lipids (i.e. GTM, SA, GMS, CP or GTL) (0.25%) melted (above 70 °C; using digital hotplate magnetic stirrer (Benchmark Scientific, UK)) in combination with one of the selected liquid lipids (IPP, PGD or GTB)

(0.75%). Aqueous phase was separately prepared using tween 80 (0.25%) and sodium taurocholate hydrate (0.25%) in water (sufficient to prepare a total of 25 ml formulation) which was preheated to 70 °C.

The drug phase containing BDP (2.6 mg) was solubilized in Soya phosphatidylcholine (0.25% and methanol (1 ml) was added to the preheated molten lipid phase, after which the preheated aqueous phase was added to the lipid phase in order to form a uniform dispersion of lipid phase through 2 min continuous stirring using magnetic stirrer (i.e. 200 RPM). The resultant micro-emulsion (oil-in-water) was subjected to probe sonication (Qsonica probe sonicator, UK) for a duration of 5 min using an amplitude intensity of 40%. BDP-NLC formulations (i.e. nano size) were successfully prepared when left to cool at room temperature (25 °C) in order to solidify solid lipid. However, the process of probe sonication caused leaching of titanium particles in BDP-NLC formulations and therefore BDP-NLC formulations were then subjected to bench centrifugation (Eppendorf centrifuge, UK) for 7 min, at a lower centrifugal force of 1500 g to remove titanium particles from NLC formulations. Such lower centrifugal force was only used to separate heavy metal i.e. titanium particles (produce during probe sonication), whereas nano particles of NLC remained suspended in the dispersion media. In terms of residual organic solvent employed in drug phase, mixing of preheated phases and their continuous stirring, followed by the use of probe sonication allowed to evaporate small volume of organic solvent from NLC formulations to avoid a possible occurrence of interdigitation and hence drug leakage.

Table 1. Composition of NLCs formulations using five solid lipids (glycerol trimyristate (GTM), stearic acid (SA), glycerol monostearate (GMS), cetyl palmitate (CP) and glycerol trilaurate (GTL)) and three liquid lipids (isopropyl palmitate (IPP), propylene glycol dicaprylate/dicaprate (PGD) and glyceryl tributyrate (GTB)) of lipid phase were used in 1:3 w/w ratios with a model drug Beclomethasone dipropionate (BDP) (2.6 mg) in order to manufacture fifteen BDP-NLC formulations. Data are mean \pm SD, n = 3

| Formulations | Liquid Lipid | Solid Lipid |
|---------------------|--|-----------------------|
| F1 | Isopropyl palmitate | Glycerol trimyristate |
| F2 | Isopropyl palmitate | Stearic acid |
| F3 | Isopropyl palmitate | Glycerol monostearate |
| F4 | Isopropyl palmitate | Cetyl palmitate |
| F5 | Isopropyl palmitate | Glyceryl trilaurate |
| F6 | Propylene glycol dicaprylate/dicaprate | Glycerol trimyristate |
| F7 | Propylene glycol dicaprylate/dicaprate | Stearic acid |
| F8 | Propylene glycol dicaprylate/dicaprate | Glycerol monostearate |
| F9 | Propylene glycol dicaprylate/dicaprate | Cetyl palmitate |
| F10 | Propylene glycol dicaprylate/dicaprate | Glyceryl trilaurate |
| F11 | Glyceryl tributyrate | Glycerol trimyristate |

| | | |
|------------|----------------------|-------------------------------|
| F12 | Glyceryl tributyrate | Stearic acid |
| F13 | Glyceryl tributyrate | Glycerol monostearate |
| F14 | Glyceryl tributyrate | Cetyl palmitate |
| F15 | Glyceryl tributyrate | Glyceryl trilaurate Trilaurin |

2.3. Size and zeta potential analysis

Particle size and polydispersity index (PDI; also denoted as size distribution) of BDP-NLC formulations were measured *via* a Zetasizer (Malvern Zetasizer Nanoseries, UK) using dynamic light scattering (DLS). Particle size was measured after preparation of BDP-NLC formulations. Moreover, post aerosolization, BDP-NLC formulation deposited in various stages of NGI were washed with deionised water, and vortexed for 1 min (Fisions WhirliMixer, Fisions Scientific Equipments, UK), followed by size analysis. Zetasizer (Malvern Zetasizer Nanoseries, UK) using Laser Doppler Velocimetry (LDV) *via* electrophoretic mobility in the dispersion medium was employed to determine Zeta potential of NLCs particles.

2.4. Entrapment efficiency

The entrapment efficiency of the BDP-NLC formulations were determined by pipetting 0.5 ml of formulation into a Millipore filter (3 kDa; Fisher Scientific, UK) and bench centrifugation (Eppendorf centrifuge, UK) was conducted for 30 min at 6,000 g. The untrapped or free drug passed through the Millipore filter, sedimenting as a filtrate at the bottom of the tube, whilst the entrapped BDP in NLCs was retained by the filter. The entrapment efficiency was identified with the help of total drug (in 1 ml of BDP-NLCs formulation) *via* HPLC.

For quantification, a HPLC (Agilent 1200 series instrument, UK) fitted with a UV detector was used with a set wavelength of 239 nm. Methanol and deionized water (75:25 v/v) were employed as a mobile phase, with a flow rate of 1.7 ml/min. An Agilent column C-18, 5 micron, 150 nm x 4.6 mm (Agilent Technology, UK) was used as a stationary phase. An injection volume of 20 µl was employed with a column temperature of 40 °C. The retention time peak was identified to appear at circa 3.7 min. Calculation of entrapment efficiency for BDP was achieved with the help of equation 1.

$$\text{Entrapment efficiency (\%)} = \frac{\text{Total drug} - \text{Untrapped drug}}{\text{Total drug}} \times 100 \quad (\text{Equation 1})$$

2.5. Morphology study *via* Transmission Electron Microscopy (TEM)

One drop of the NLC formulation and one drop of negative stain i.e. phosphotungstic acid 1% were combined, transferred onto a carbon coated copper grid (400 mesh) (TAAB Laboratories Equipment Ltd., UK) and allowed to dry for 30 min. Samples were placed in the TEM instrument (Morgagni 268, MegaView, UK) and morphology of BDP-NLC formulations were observed and images were captured at various magnifications.

2.6. NLC formulations stability studies

Suspension of BDP-NLC formulations were characterized for particle size and PDI using three different temperature conditions, in order to analyse potential particle aggregation/fusion. Formulations were stored in a glass bottle (25 ml) for six weeks at 4, 25 and 45 °C. These conditions were kept constant throughout the stability studies. Particle size and PDI were determined in accordance to section 2.3.

2.7. NLCs deposition in Next generation impactor (NGI) *via* medical nebulizers

Pre-operation, all equipment components along with stages of the NGI (Copley Scientific, UK) were washed with methanol and allowed to dry. Stages for sample collection/deposition were not sprayed with silicon or surfactant fluid according to European Pharmaceutical Aerosol Group (EPAG) for nebulizers. The NGI was coupled with a Copley TPK 2000 critical airflow controller and a Copley HCP5 vacuum pump (Copley Scientific, UK), and airflow was adjusted to 60 or 15 L/min. According to the specifications of European Pharmacopoeia (i.e. Chapter 2.9.44), the NGI with its collection stages and induction port were placed in refrigerator at 5 °C for 90 min prior to use. Three different types of nebulizers were employed for this study including; Air jet nebulizer (PARI Turboboy 5 air jet, UK), Vibrating mesh nebulizer (Omron Micro-air U22 pocket nebulizer, UK), and Ultrasonic nebulizer (Unicliffe rechargeable ultrasonic inhaler MY-520B, UK). The empty stages and empty nebulizer were separately weighed pre nebulization. BDP-NLC formulations (5 ml) were pipetted into the nebulizer reservoir and the weight of 5 ml of formulation recorded. The nebulizer was aligned with the throat section (i.e. induction port) of the NGI before switching on the aerosolization through nebulizer, flow pump and timer. Pre-separator was not used during nebulization, as the generated droplets easily moved into the NGI stages (without blocking NGI stages) and deposited in their respective stages (based on their droplets size). Whereas, pre-separator is important for dry powder inhalers in order to separate lumps or very large particles due to their gravity and to avoid blockage of NGI stages (Marple et al., 2004). Post nebulization, the amount of formulation

deposited onto each stage was determined. It is noteworthy that nebulizers deliver large doses when compared to other types of inhalation devices, making gravimetric technique more valid for such studies. Other investigators within the same research filed also used this technique (Sweeney et al., 2019, Morin et al., 2014, Ung et al., 2014).

After achieving nebulization to 'dryness', complete nebulization time was determined, which is the time required from aerosol generation to complete cessation of aerosol formation. Aerosol mass output was determined by calculating the percentage of aerosol mass deposited in various stages of NGI. Whereas, output rate was calculated gravimetrically by determining the amount/volume of formulation generated per min. Both aerosol mass output (Equation 2) and output rate (Equation 3) were determined.

$$\text{Mass output (\%)} = \left(\frac{\text{Weight of nebulized formulation}}{\text{Weight of formulation present in the nebulizer prior to nebulization}} \right) \times 100 \quad (\text{Equation 2})$$

$$\text{Aerosol output rate (mg/min)} = \left(\frac{\text{Weight of nebulized formulation}}{\text{Complete nebulization time}} \right) \quad (\text{Equation 3})$$

When using the 60 L/min airflow rate using the NGI, the aerodynamic cut-off diameter for each stage was calibrated by the manufacturer and stated as Stage 1 (8.06 μm); Stage 2 (4.46 μm); Stage 3 (2.82 μm); Stage 4 (1.66 μm); Stage 5 (0.94 μm); Stage 6 (0.55 μm); Stage 7 (0.34 μm) and Micro-orifice collector (MOC) (<0.34 μm). Similarly, for 15 L/min airflow rate, the cut-off diameter was calibrated for each stage and stated as follows: Stage is stated as Stage 1 (14.10 μm); Stage 2 (8.61 μm); Stage 3 (5.39 μm); Stage 4 (3.30 μm); Stage 5 (2.08 μm); Stage 6 (1.36 μm); Stage 7 (0.98 μm) and MOC (<0.70 μm). Aerosol deposition in the various stages of NGI were also calculated for fine particle dose (FPD), fine particle fraction (FPF) and respirable fraction (RF).

FPD is the mass of particles <5 μm in size within the total emitted dose. This refers to formulation deposited on stages 2 to 7 for 60 L/min, representing cut-off sizes at 4.46 to 0.34 μm ; and stages 4 to 7 for 15 L/min airflow rate demonstrating cut-off sizes at 3.30 to 0.98 μm in the NGI respectively. FPF is the fraction of particles <5 μm related to the emitted mass. RF is generally considered as the fraction of an aerosol contained particle that are <5 μm aerodynamic diameter and was expressed as the percentage of FPD (deposition of formulation on stage 2 – 7 and 4 – 7 for 60 and 15 L/min, respectively) to the total deposition on all stages (i.e. 1 – 8). Additionally, the mass median aerodynamic diameter (MMAD) of aerosol particle and geometric standard deviation (GSD) were also calculated using Copley Inhaler Testing Data Analysis Software (CITDAS) Version 3.10.

2.8. Statistical analysis

Statistical analysis was performed on the data obtained using Student's *t*-test by the use of the SPSS software. This was done to determine if there was any significant difference between any two groups of data or sets of data, respectively. All experimental were conducted in triplicate using three different batches, and the difference was deemed to be statistically significant when the resulting *p* value was lower than 0.05.

3. Results and discussion

3.1. Initial investigation and formulations selection

Initial investigations of BDP-NLC formulations were conducted with regards to particle size, PDI, Zeta potential and entrapment efficiency when freshly prepared, as well as when stored for one week (i.e. 25 °C). It was found that BDP-NLC formulations prepared containing liquid lipids i.e. IPP (i.e. F1 – F5) or GTB (i.e. F11 – F15) resulted in particle aggregation, and thus a significant difference in particle size ($p < 0.05$) was found between freshly prepared BDP-NLC formulations when compared to formulations stored for one week; the latter being larger (Table 2). Comparatively, BDP-NLCs formulation prepared with PGD as a liquid lipid exhibited greater stability (high stability against oxidation), with no significant difference ($p > 0.05$) observed in terms of particle size, with the exceptions of the F6 and F9 formulations, where the solid lipid component (i.e. GTM and CP) may be responsible for the larger particle size observed. The addition of Miglyol 840 (i.e. PGD) as a liquid lipid in BDP-NLC formulations may enable emulsification and hence prevent particle aggregation (Mahant et al., 2018). It was also reported by Barbosa et al. (2016) that Miglyol 840 (i.e. PGD) as a liquid lipid reduces particle crystallinity, as well as supporting formulation stability due to lattice deformation in the lipid core, resulting in greater stability. The difference in particle size when employing IPP and GTB were also attributed to particle aggregation. Similar to particle size, formulations F1 – F6, F9 and F11 – F15 also exhibited larger PDI. This may further confirm the presence of particle aggregation, as PDI was increased due to aggregation (Table 2).

Moreover, no significant difference ($p > 0.05$) was found in Zeta potential values between freshly prepared and after one week stability of BDP-NLC formulations (Table 2). Similar to Zeta potential values, no significant difference ($p > 0.05$) was observed in terms of entrapment efficiencies between the tested formulations (Table 2). In literature, a number of various combinations of solid to liquid lipids (i.e. 99.9:0.1 – 25:75) have been reported, where solid lipid was mostly employed in higher concentration than liquid lipid (Cao et al., 2019, Weber et

al., 2014). High entrapment efficiency of BDP observed in the BDP-NLC formulations may be attributed to the presence of liquid lipid, readily miscible with others oils and surfactants. The high proportion of liquid lipid may cause immense disorder in the crystal lattice, allowing greater BDP accommodation improving and enhancing BDP solubility in the lipid matrix (offering very good solubility characteristics), leading to high drug entrapment (i.e. 87 – 94%). Moreover, the high portion of liquid lipid in addition to solid lipids may result in imperfections within the crystal matrix and therefore providing sufficient space for active molecule to lodge into. This phenomena was also observed in the studies conducted by Hu et al. (2006) and Kelidari et al. (2017), where high entrapment was observed upon increasing liquid lipid concentration when compared to solid lipid in NLC formulations. These results are also in concordance with the previous research conducted by Shah et al. (2016) and Thatipamula et al. (2011) for high drug entrapment. In general, it was observed that higher liquid lipid concentration might be responsible for smaller particle size and high drug entrapment. Overall, based on the discussed characterization, the following formulations were selected for further studies; F7, F8 and F10.

Table 2: Particle size, polydispersity index (PDI), Zeta potential and entrapment efficiency of Beclomethasone dipropionate (BDP) of freshly prepared BDP-NLC formulations (F1 – F15), as well as after one week of stability at 25 °C. Data are mean \pm SD, n = 3

| Formulation S | Size (nm) | | PDI | | Zeta potential (mV) | | Entrapment efficiency (%) | |
|---------------|-------------------|--------------------|-------------------|--------------------|---------------------|--------------------|---------------------------|--------------------|
| | After preparation | 25 °C after 1 week | After preparation | 25 °C after 1 week | After preparation | 25 °C after 1 week | After preparation | 25 °C after 1 week |
| F1 | 226.31 \pm 5.57 | 285.52 \pm 6.34 | 0.29 \pm 0.01 | 0.45 \pm 0.02 | -4.31 \pm 1.02 | -4.66 \pm 1.36 | 94.26 \pm 4.32 | 92.51 \pm 4.76 |
| F2 | 201.54 \pm 6.21 | 255.31 \pm 5.71 | 0.26 \pm 0.01 | 0.59 \pm 0.03 | -8.26 \pm 1.54 | -9.74 \pm 2.03 | 93.73 \pm 5.24 | 91.75 \pm 5.61 |
| F3 | 436.30 \pm 4.33 | 477.26 \pm 4.68 | 0.45 \pm 0.03 | 0.75 \pm 0.05 | -7.36 \pm 1.28 | -9.67 \pm 2.51 | 94.33 \pm 6.42 | 91.79 \pm 4.91 |
| F4 | 245.18 \pm 6.25 | 269.85 \pm 5.27 | 0.41 \pm 0.03 | 0.58 \pm 0.03 | -13.64 \pm 2.81 | -15.72 \pm 3.17 | 94.07 \pm 5.16 | 93.57 \pm 4.83 |
| F5 | 244.19 \pm 7.26 | 493.88 \pm 7.61 | 0.34 \pm 0.03 | 0.77 \pm 0.06 | -6.39 \pm 1.82 | -8.06 \pm 2.61 | 90.08 \pm 5.77 | 89.74 \pm 5.37 |
| F6 | 253.18 \pm 5.16 | 268.15 \pm 5.06 | 0.43 \pm 0.03 | 0.58 \pm 0.02 | -6.79 \pm 1.34 | -5.18 \pm 1.06 | 93.52 \pm 6.05 | 90.73 \pm 5.71 |
| F7 | 241.20 \pm 5.73 | 239.55 \pm 5.06 | 0.24 \pm 0.03 | 0.24 \pm 0.02 | -4.27 \pm 1.02 | -3.55 \pm 1.06 | 96.88 \pm 4.76 | 94.37 \pm 4.06 |
| F8 | 233.41 \pm 4.38 | 228.97 \pm 5.53 | 0.26 \pm 0.02 | 0.23 \pm 0.02 | -3.54 \pm 0.98 | -3.44 \pm 0.87 | 95.64 \pm 4.39 | 91.38 \pm 5.03 |
| F9 | 244.35 \pm 6.05 | 283.58 \pm 8.01 | 0.36 \pm 0.01 | 0.52 \pm 0.04 | -4.92 \pm 1.17 | -3.65 \pm 1.12 | 94.46 \pm 5.28 | 92.46 \pm 5.61 |
| F10 | 223.69 \pm 5.51 | 217.87 \pm 6.34 | 0.26 \pm 0.02 | 0.25 \pm 0.02 | -1.36 \pm 0.06 | -1.24 \pm 0.07 | 94.56 \pm 6.44 | 91.92 \pm 5.39 |
| F11 | 245.24 \pm 8.15 | 313.63 \pm 7.74 | 0.36 \pm 0.01 | 0.63 \pm 0.04 | -8.81 \pm 2.37 | -8.23 \pm 1.86 | 92.68 \pm 6.62 | 88.97 \pm 5.44 |
| F12 | 262.65 \pm 7.25 | 308.53 \pm 6.81 | 0.26 \pm 0.03 | 0.64 \pm 0.03 | -12.64 \pm 3.16 | -10.83 \pm 2.76 | 93.54 \pm 5.70 | 90.17 \pm 4.71 |
| F13 | 270.45 \pm 5.67 | 294.21 \pm 6.62 | 0.31 \pm 0.02 | 0.58 \pm 0.02 | -14.59 \pm 4.35 | -11.84 \pm 3.43 | 90.16 \pm 4.94 | 87.26 \pm 5.87 |
| F14 | 257.91 \pm 5.59 | 324.26 \pm 7.18 | 0.34 \pm 0.03 | 0.61 \pm 0.04 | -12.66 \pm 3.71 | -12.55 \pm 3.65 | 93.34 \pm 5.48 | 90.59 \pm 6.31 |
| F15 | 339.64 \pm 5.64 | 379.23 \pm 6.26 | 0.53 \pm 0.03 | 0.73 \pm 0.05 | -5.49 \pm 1.31 | -7.64 \pm 1.66 | 90.09 \pm 5.51 | 93.46 \pm 5.94 |

3.2. Morphology study *via* transmission electron microscopy (TEM)

Surface morphology of BDP-NLC particles were examined for all three formulations (F7, F8 and F10). NLC particles were confirmed to be within the nanometre size range as well as spherical in shape (Figure 1). Additionally, a low PDI of the BDP-NLC formulation examined was observed confirming uniformity in terms of size. Similar observations in terms of surface morphology were also reported by Shah et al. (2016) (Table 2).

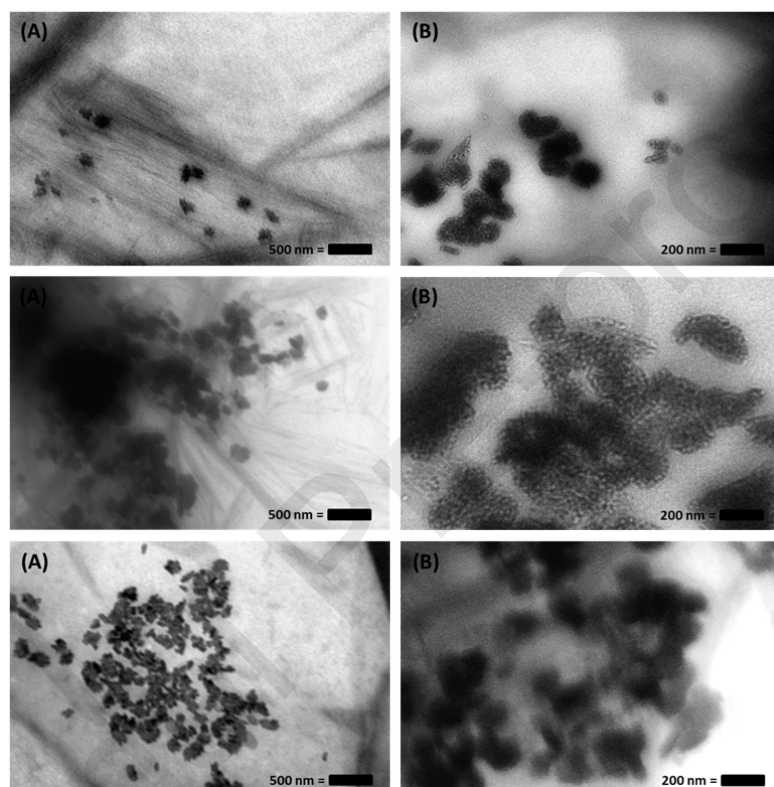


Figure 1: TEM images of BDP-NLC (A and B) F7, (C and D) F8 and, (E and F) F10 formulations with two different magnifications. These images are typical of three such different experiments

3.3. BDP-NLCs particle size in NGI stages

Based on aforementioned characterization (Section 3.1), selected BDP-NLC formulations (i.e. F7, F8 and F10) were aerosolized where the airflow suction was conducted at 60 L/min using all three nebulizers (i.e. Air jet, Vibrating mesh and Ultrasonic) through the NGI. The deposited aerosol droplets containing BDP-NLC particles in various stages were analysed in terms of their particle size. Prior to aerosolization, BDP-NLCs particle size of formulations F7, F8 and F10 were 241.20 ± 5.73 , 233.41 ± 4.38 and 223.69 ± 5.51 nm, respectively (Table 2). Post

nebulization, a general trend of decreasing particle size was observed from stage 1 to stage 8 for all three formulations using all three nebulizers (Figure 2). Stage 1 of the NGI demonstrated a greater degree of particle deposition, which may potentially be associated with the impaction properties of aerosol droplets (i.e. related to the poor manoeuvrability). This may be also related to the various cut-off diameters between each stage of NGI, resulting in larger droplets/particle deposition in the initial stages and deposition of finer droplets/particles in the latter NGI stages.

Upon analysis, it was found that F10 formulation exhibited greater stability and consistency in terms of particle size when compared to F7 and F8 formulations. This trend was clearly observed in stages 1 and 2, where the particle size of F10 formulation was observed to be significantly smaller ($p < 0.05$) for all three nebulizers when compared to F7 and F8 formulations (Figure 2). Additionally, shear forces generated in nebulizers during the nebulization process insignificantly influenced the F10 formulations, demonstrating most stable and reliable formulation.

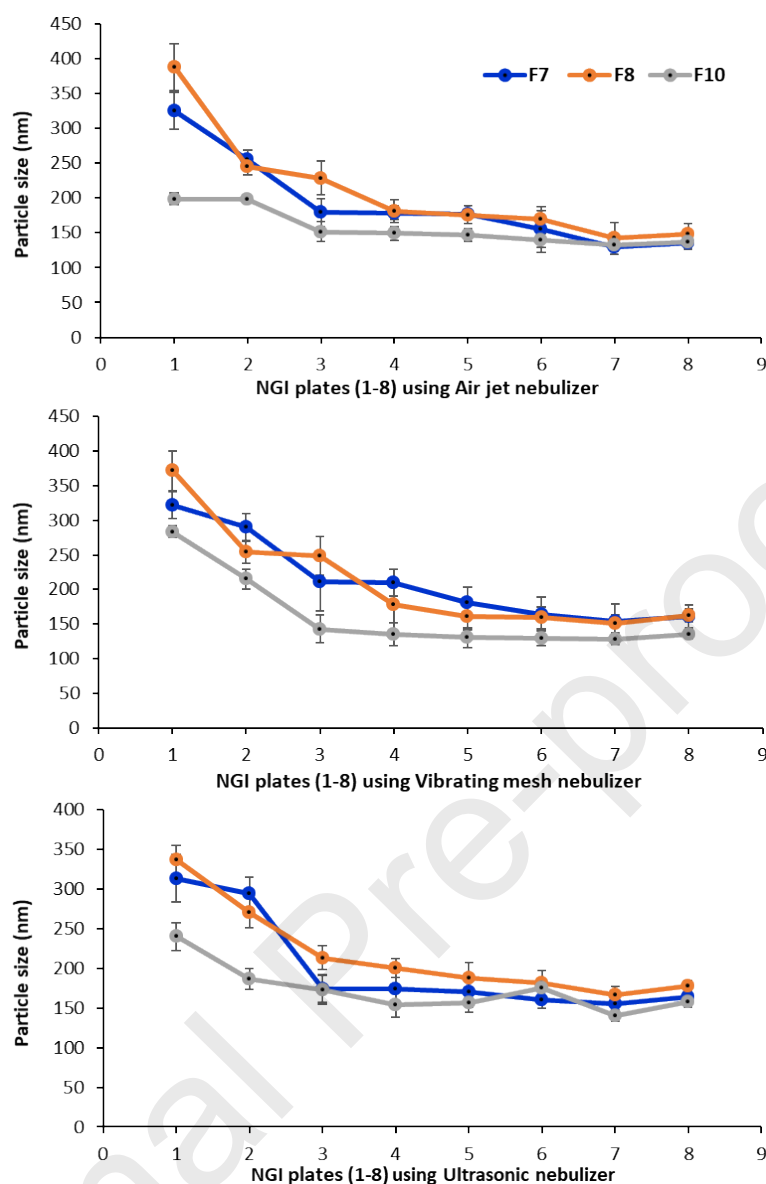


Figure 2: Deposition of aerosol droplets containing BDP-NLC particles in various stages of NGI (i.e. 1 – 8) using formulations F7, F8 and F10 after aerosolization using 60 L/min employing an Air jet, Vibrating mesh and Ultrasonic nebulizers. Data are mean \pm SD, n = 3

3.4. Stability studies of BDP-NLC formulations

Selected F7, F8 and F10 BDP-NLC formulations were further characterized for their stability studies using three different temperature conditions (i.e. 4, 25 and 45 °C) for six weeks. Upon analysis of BDP-NLC formulations after two, four and six weeks; it was identified that at 4 °C, particles size was significantly increased ($p < 0.05$) for formulations F7 (2.8, 3.1 and 3.0 times) and F8 (1.7, 1.8 and 1.9 times) when compared to freshly prepared F7 and F8 formulations (i.e. 241.20 ± 5.73 nm and 233.41 ± 4.38 nm) (Table 3 and Table 2). Particle size of formulations F7 and F8 remained stable for four weeks at 25 °C, however a significant increase ($p < 0.05$) in particle size was noted at week six for both formulations (Table 3). Moreover,

particle size at 45 °C remained stable throughout the period of stability studies for all three formulations. This may be associated with elevated stability temperature, which may least affected solid lipids in the NLCs formulations.

BDP-NLCs formulation F7 (containing SA as a solid lipid) exhibited significantly larger ($p < 0.05$) particle size at 4 °C, causing particle aggregation. Similar findings were also reported by Kelidari et al. (2017), where the size of particles containing SA significantly increased when stored at 4 °C, when compared to freshly prepared particles. Whereas, the same formulation remain unchanged in first two weeks but significantly increased in size after one month as well as PDI when kept at 25 °C (Shafique et al., 2017). Similar trend was also seen in the present study, where particles were significantly increased at 4 °C, whereas particles at 25 °C remain unchanged initially (after four weeks) but significantly increased ($p < 0.05$) after week six from the freshly prepared particles size (Table 3). Analogous to this study, BDP-NLCs F7 formulation demonstrated no significant change in particle size at 45 °C, which was also observed by Sahito et al. (2020).

BDP-NLCs formulation F8 containing GMS, present as a solid lipid demonstrated sensitivity towards particle size at 4 °C and hence showed particle aggregation/growth after six weeks (Table 3). This was also confirmed by El-Salamouni et al. (2015), where particle size significantly increase after two weeks, exhibiting the existence of structural changes upon melting and congealing. In the current study particle size gradually but significantly increased ($p < 0.05$) after four and six weeks when kept at 25 °C than the freshly prepared particle size (Table 3). Similar findings were also reported by Makoni et al. (2019), where NLCs particles containing formulation GMS as a solid lipid increased after two, four and eight weeks. BDP-NLC formulations at stability temperature of 45 °C, showed an insignificant change in particle size after four week, which was also confirmed by the previous research conducted by Kumar et al. (2013).

Mirroring particle size, an increased in particle size distribution for both F7 and F8 formulations was also observed, indicating a wide size distribution overall. However, for the F10 BDP-NLCs formulation, no significant change ($p > 0.05$) in PDI was observed during stability studies (Table 3).

Table 3: Particle size and particle size distribution (i.e. PDI) of BDP-NLC F7, F8 and F10 formulations after two, four and six week of stability studies using three different temperature conditions (i.e. 4, 25 and 45 °C). Data are mean \pm SD, n = 3

| Formulations | F7 | | F8 | | F10 | |
|--------------|-----------|-----|-----------|-----|-----------|-----|
| | Size (nm) | PDI | Size (nm) | PDI | Size (nm) | PDI |

| Week 2 | | | | | | |
|---------------|---------------|-------------|---------------|-------------|---------------|-------------|
| 4 °C | 676.45 ± 8.54 | 0.85 ± 0.13 | 408.41 ± 6.15 | 0.65 ± 0.09 | 220.65 ± 5.86 | 0.22 ± 0.06 |
| 25 °C | 247.63 ± 5.94 | 0.36 ± 0.09 | 234.81 ± 4.64 | 0.29 ± 0.07 | 219.43 ± 6.28 | 0.24 ± 0.08 |
| 45 °C | 245.65 ± 4.67 | 0.28 ± 0.06 | 231.59 ± 5.73 | 0.29 ± 0.08 | 225.76 ± 7.07 | 0.23 ± 0.09 |
| Week 4 | | | | | | |
| 4 °C | 737.81 ± 9.79 | 0.97 ± 0.18 | 423.67 ± 6.63 | 0.68 ± 0.11 | 227.28 ± 6.35 | 0.21 ± 0.05 |
| 25 °C | 251.79 ± 6.56 | 0.39 ± 0.11 | 246.54 ± 6.63 | 0.31 ± 0.09 | 217.74 ± 7.15 | 0.25 ± 0.09 |
| 45 °C | 246.1 ± 6.72 | 0.27 ± 0.08 | 233.82 ± 4.08 | 0.31 ± 0.10 | 218.27 ± 6.58 | 0.27 ± 0.11 |
| Week 6 | | | | | | |
| 4 °C | 727.97 ± 9.16 | 0.99 ± 1.15 | 439.83 ± 7.28 | 0.67 ± 0.13 | 232.42 ± 6.61 | 0.22 ± 0.07 |
| 25 °C | 278.58 ± 7.25 | 0.43 ± 0.11 | 265.22 ± 5.83 | 0.37 ± 0.08 | 226.49 ± 7.86 | 0.27 ± 0.08 |
| 45 °C | 248.18 ± 5.91 | 0.29 ± 0.06 | 236.72 ± 5.37 | 0.35 ± 0.12 | 221.98 ± 7.13 | 0.26 ± 0.08 |

BDP-NLCs formulation F10, did not elicit any significant change ($p > 0.05$) in size and PDI from the freshly prepared samples ($223.69 \pm 5.51 \text{ nm}$), when stability studies were conducted using three different temperatures (Table 3). This might be associated with the more stable form of the solid lipid used (i.e. GTL). A study conducted by Olbrich et al. (2002) demonstrated that GTL retains stability at cold temperatures ($4 \text{ }^\circ\text{C}$) in disperse formulation/system, offering an explanation behind the stability of the F10 formulation remain at cold temperature, with no further increase in particles size observed. The melting point of GTL (i.e. circa $46 \text{ }^\circ\text{C}$) is close to the stability temperature of $45 \text{ }^\circ\text{C}$, thus the elevated temperature condition did not impact upon the physical stability of the F10 formulation. Moreover, based on the two extreme temperature conditions (i.e. 4 and $45 \text{ }^\circ\text{C}$), it was noted that the BDP-NLCs F10 formulation with solid lipid GTL, remained stable at room temperature and hence no significant change ($p > 0.05$) was observed in particles size (Table 3). Similar reports were observed by Saupe et al. (2005), which indicated that NLCs formulations are more stable at room temperature.

Overall, the BDP-NLCs F10 formulation exhibited higher stability under various temperature conditions, as well as particle size deposition in the various stages of the NGI (Section 3.3). This formulation (F10) was thus selected for further characterization and nebulization performance.

3.5. Nebulizer performance *via* deposition of BDP in various stages of NGI using two different airflow rates

Upon aerosolization (60 and 15 L/min) of formulation F10 using all three nebulizers, the Air jet nebulizer demonstrated lower deposition of the BDP formulation in the initial stages, and higher deposition in the lateral stages of the NGI, which is significantly different ($p < 0.05$) to the alternative two nebulizers investigated (i.e. Vibrating mesh and Ultrasonic) (Figure 3). This suggests that highly compressed air paired with high velocity results in the deposition of larger droplets (containing BDP-NLC particles of small mass) in the initial stages, whereas, high deposition of smaller droplets/particles are propelled in the NGI to the lateral stages at both 60 and 15 L/min; thus improve deep lung deposition. Moreover, it is suggested that at lower airflow rate of 15 L/min (i.e. low inlet velocity), the F10 formulation paired with the Air jet nebulizer deposited a smaller mass ($p < 0.05$) of formulation in the initial stages (1 – 4) of the NGI and higher in the lateral stages.

The Vibrating mesh nebulizer demonstrated significantly higher BDP formulation deposition in the initial stages ($p < 0.05$) than in the lateral stages, at airflow rate of 60 L/min; whereas, at 15 L/min airflow rate, a consistent increase of BDP deposition was found till stage 5, followed by a consistent drop of BDP deposition in the following stages (Figure 3). This may be related to the inertial impaction mechanism of particle deposition, where high inlet velocity (i.e. 60 L/min) may retard particles manoeuvring ability during aerosolization between the various stages of NGI (due to cut-off diameter), leading to higher BDP deposition in the initial stages, particularly the first 2 stages (at higher airflow rate i.e. 60 L/min). Contrastingly, at a lower airflow rate (i.e. 15 L/min) lower BDP deposition was found in the initial two stages of NGI.

For the Ultrasonic nebulizer at 60 L/min, it was noticed that high degree of BDP formulation deposited in the initial stages and lower in the later stages (the opposite to deposition observed in the Air jet nebulizer). Whereas at 15 L/min, a smaller mass of formulation was deposited in the initial stages and higher at the lateral stages, which again related to the inlet velocities generated during aerosolization (Figure 3).

It was suggested that at 60 L/min airflow rate, the high velocity of air inlet through NGI allowed for higher deposition in the initial stages for both Vibrating mesh and Ultrasonic nebulizers due to inertial impaction, as particles manoeuvring was compromised *via* high inlet airflow and therefore a lower BDP was deposited in the lateral stages. However, the same nebulizers and formulation at a lower airflow rate of 15 L/min exhibited low formulation deposition in the initial stages and higher in the middle to lateral stages, suggesting that droplets were not influenced by the inertial impaction, as low inlet airflow allowed the droplets to manoeuvre the NGI, with the majority of the BDP formulations depositing in the middle to later stages. Amongst all three nebulizers, the Air jet nebulizer exhibited the highest formulation deposition in the middle to

lateral stages of the NGI at both 60 and 15 L/min airflow rates, suggesting greater nebulization performance.

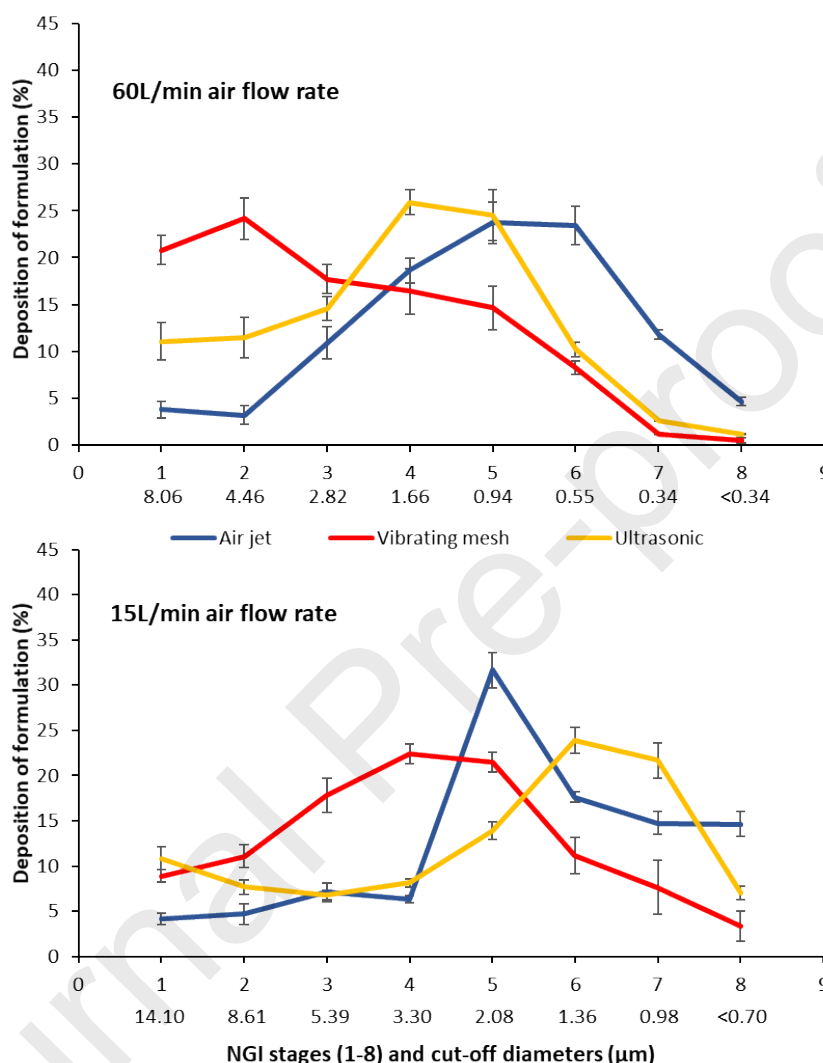


Figure 3: Showing deposition of BDP of NLCs F10 formulation in various stages i.e. 1 – 8 of the NGI (with the cut-off diameter of each stage in µm). Three nebulizers, including Air jet, Vibrating mesh and Ultrasonic were denoted as horizontal lines with error bars for formulation deposition (post aerosolization) using two different airflow rates i.e. 60 and 15 L/min. Data are mean ± SD, n = 3

3.6. Nebulization time of F10 formulation via three nebulizers using two different airflow rates

Nebulization time is the total time required for the formulation to aerosolize. Overall, the Vibrating mesh and Ultrasonic nebulizers elicited significantly ($p < 0.05$) shorter nebulization times when compared to the Air jet nebulizer, irrespective of airflow rate (Figure 4). However,

upon comparison to each other, both the Vibrating mesh and Ultrasonic nebulizers exhibited no difference ($p>0.05$) in nebulization time, irrespective of airflow rate. However, both demonstrated shorter nebulization times ($p<0.05$) when a 60 L/min airflow rate was utilised.

It is proposed that the Air jet nebulizer uses high compressed air, which generates shear forces creating a negative pressure, converting the liquid formulation into aerosol *via* the aid of the venture and baffle (baffle located right above venture). During aerosolization, larger droplets impact upon the baffle, dispersing into smaller droplet and thus allowing for the generation of finer droplet aerosols for inhalation. This process may also result in sticking of the formulation to the baffle as well as side walls, which are deflected back (i.e. taking extra time) into the nebulizer reservoir for further atomization into smaller inhalable droplets (Khan et al., 2016). Additionally, the generation of aerosol *via* compressed air through venture may lead to foam formation, which is related to the presence of surfactants in the NLCs formulation (tween 80 and sodium taurocholate hydrate). It is suggested that irrespective of airflow rate (i.e. high or low for suction of generated aerosol droplets through NGI), formulation conversion into aerosols and formulation deflection back into nebulizer reservoir remain consistent and hence formulation take longer nebulization time (Figure 4). Elevated Air jet nebulization time may also be related to the lowering of formulation temperature in the nebulizer reservoir, which increases formulation viscosity, reducing nebulizer output as well as reduces the conversion of aerosolization process from the NLCs formulation in the nebulizer reservoir (O'Callaghan and Barry, 1997, Khan et al., 2016, Khan et al., 2020c, Beck-Broichsitter et al., 2012). Elevated nebulization time when using Air jet nebulizers were also demonstrated by Elhissi et al. (2007). This is further confirmation that the Air jet nebulizer produces smaller aerosol droplets; as a result reduced formulation deposition occurs in the initial stages and higher deposition in the middle to lateral stages of NGI (Section 3.5), regardless of airflow rate (Figure 3).

Airflow was identified as the overriding factor for nebulization time when using either a Vibrating mesh or Ultrasonic nebulizer (Figure 4). Both Vibrating mesh and Ultrasonic nebulizer use piezoelectric crystals, which vibrate generating aerosols. In the Vibrating mesh nebulizer, a perforated mesh plate allows for the generation and release of aerosol, whereas in an Ultrasonic nebulizer, vibration frequency produced *via* a piezoelectric crystal enables aerosol formation. Upon generation of aerosol from Vibrating mesh and Ultrasonic nebulizers, high and low airflow rate immediately draw up the aerosol, offering limited chances of formulation deflection (in contrast to Air jet nebulizer) and hence the formulation requires a shorter nebulization time (i.e. ~30 and ~28 min at 60 L/min; and, 36 and 29 min at 15 L/min for Vibrating mesh and Ultrasonic nebulizers respectively) (Figure 4).

Overall, Air jet nebulizer demonstrated longer nebulization time, when compared to the counterparts tested, however this may be beneficial in terms of drug deposition for prophylaxis purposes (i.e. high concentrations reaching the latter stages of the NGI) using normal tidal breathing (Section 3.5 and 3.6).

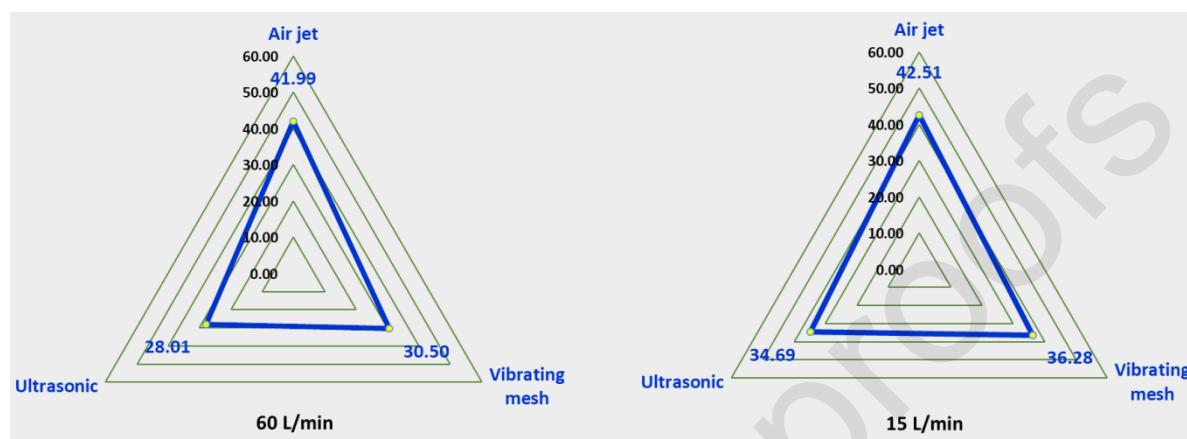


Figure 4: Nebulization time of BDP-NLCs F10 formulations using three nebulizers (i.e. Air jet, Vibrating mesh and Ultrasonic) employing two airflow rates i.e. 60 and 15 L/min. Data are mean \pm SD, n = 3

3.7. Mass output and output rate of F10 formulation via three nebulizers using two different airflow rates

Mass output is the term used for the total nebulized formulation to dryness (expressed in percentage). In general, no significant difference was observed for mass output between both airflow rates (i.e. 60 and 15 L/min) for suction of aerosol droplets (Figure 5). The following trend in terms of mass output was observed amongst the nebulizers tested; Vibrating mesh > Air jet > Ultrasonic nebulizer. Significantly higher ($p < 0.05$) mass output was exhibited by the Vibrating mesh nebulizer (at both airflow rates), demonstrating most of the formulation release from the nebulizer (~97%) (Figure 5), whereas, the Air jet and Ultrasonic nebulizer exhibited an average of about 85% and 77% aerosol mass output using 60 and 15 L/min airflow rates (Figure 5). The lower mass output of NLC F10 formulation by the Ultrasonic nebulizer may be attributed to the high residual volume (also known as dead volume), as well as heat generation in the nebulizer reservoir (Rau, 2002, Khan et al., 2016, Phipps and Gonda, 1990, Dhand, 2008), causing NLC particle aggregation/fusion. It is noteworthy that irrespective of complete nebulization time, 100% mass output cannot be achieved, as a fraction of the formulation will remain in the nebulizer reservoir as dead or residual volume (Hess et al., 1996, Khan et al., 2020a, Elhissi et al., 2007).

Higher mass output by Vibrating mesh nebulizer may be suggestive that the mesh nebulizer may be more appropriate for disperse systems and solutions containing smaller particles (Dhand, 2002). Additionally, the design of reservoir in mesh nebulizer has a slanted position, which allows for maximum flow of formulation towards the perforated plate for aerosolization. This process facilitates maximum aerosol formation, with little formulation adhering to the nebulizer reservoir as well as deflection back into the nebulizer reservoir. A similar trend in mass output using all three nebulizers (Vibrating mesh > Air jet > Ultrasonic) was also reported by Elhissi and Taylor (2005). Mass output observed in the current research corresponds to previous research, where a smaller volume of formulation remains in the reservoir of the Vibrating mesh nebulizer post nebulization, when compared to Air jet and Ultrasonic nebulizer (Dhand, 2002, Ismail and Chrystyn, 2004). Overall, both the Vibrating mesh and Air jet nebulizers were found to be dominant in terms of mass output.

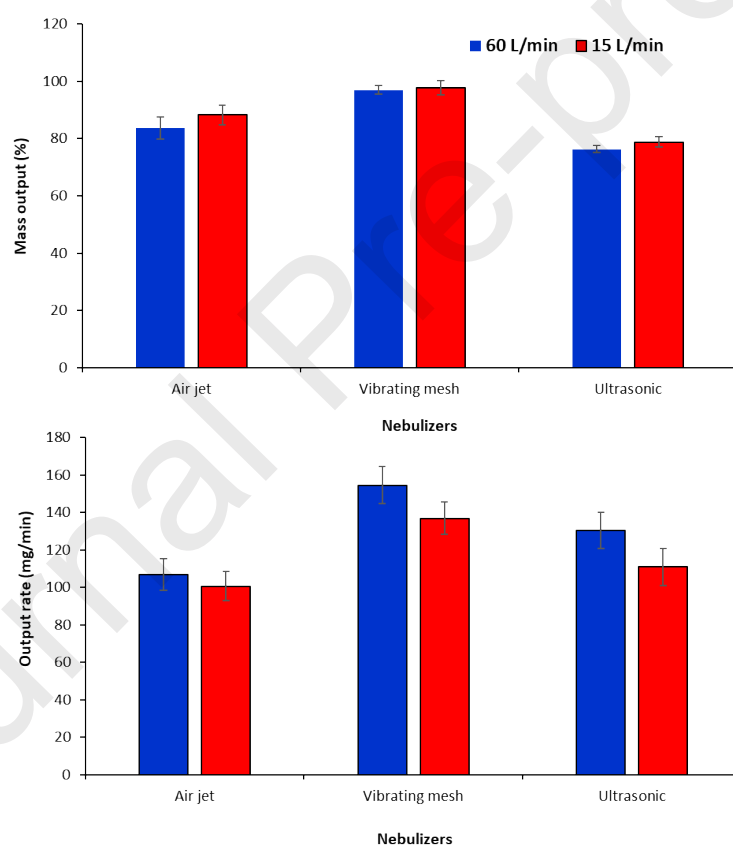


Figure 5: Mass output and output rate of BDP-NLCs F10 formulations after aerosolization using three nebulizers (i.e. Air jet, Vibrating mesh and Ultrasonic) employing two different airflow rates i.e. 60 and 15 L/min. Data are mean \pm SD, n = 3

The output rate of BDP-NLCs F10 formulation remained consistent irrespective of airflow rates when employing all three nebulizers (Figure 5). Upon investigation of output rate, regardless of both airflow rates, the Vibrating mesh nebulizer exhibited the highest output rate (average

of ~145 mg/min), this was followed by the Ultrasonic nebulizer (average output rate of ~120 mg/min), whereas the Air jet nebulizer exhibited the lowest output rate (Figure 5). Output rate exhibited by nebulizers is directly related to nebulization time; the longer the nebulization time, the lower the output rate. Similar findings of high nebulization time and lower aerosol output rate was also reported in the literature using NLCs formulations (Nafee et al., 2018) as well as other lipid-based formulations (Elhissi et al., 2007, Khan et al., 2020a).

Overall, at both airflow rates of 60 and 15 L/min, the Vibrating mesh nebulizer generated aerosol with higher mass and output rates than both the Air jet and Ultrasonic nebulizers (Figure 5). Additionally, whilst the Vibrating mesh nebulizer contains a perforated plate, this was not observed to hinder the BDP-NLCs formulation, as the pores in perforated plate are 3 μm in size and around 6000 in number (Khan et al., 2013, Elhissi et al., 2007); NLC particle size was observed to ~225 nm (Table 2). Thus the Vibrating mesh nebulizer completed nebulization time to dryness in much shorter time when compared to Air jet nebulizer (Figure 4), as a result, higher mass output and output rate was achieved by Vibrating mesh nebulizer than the other counterparts (Figure 5).

3.8. Fine particle dose (FPD), fine particle fraction (FPF) and respirable fraction (RF) of NLCs F10 formulation

Upon analysis, FPD showed higher BDP deposition in the following trend using various nebulizers for BDP-NLCs F10 formulation; Air jet > Vibrating mesh > Ultrasonic nebulizer (Table 4). For the 60 L/min airflow rate, higher BDP deposition was found for Air jet and Vibrating mesh nebulizer (90.45 ± 5.47 and 84.15 ± 4.36 μg), whereas significantly lower ($p < 0.05$) deposition in the NGI stages was observed for the Ultrasonic nebulizer (36.53 ± 3.69 μg). A similar trend for formulation deposition was also exhibited at the lower airflow rate (i.e. 15 L/min), albeit significantly lower overall (Table 4). Higher FPD exhibited by the Air jet and Vibrating mesh nebulizers may be associated with the lower residual volume remaining in the nebulizer reservoir after complete aerosolization. Fine particle fraction (FPF) refers to the fraction of particles smaller than 5 μm related to the emitted mass. Trends in deposition observed in FPD were mirrored in FPF. FPF was observed to be higher ($p < 0.05$) for the Air jet and Vibrating mesh nebulizers when compared to the Ultrasonic nebulizer (Table 4). Similarly, higher FPF was also reported by Abdelrahim (2011) and Abdelrahim et al. (2010) for both Jet and Vibrating mesh nebulizers using lipid-based formulations.

Table 4: Aerosol dispersion performance parameters including; fine particle dose (FPD), fine particle fraction (FPF), respirable fraction (RF), mass median aerodynamic diameter (MMAD) and geometric standard deviation (GSD) of BDP-NLCs F10 formulation using three nebulizers (i.e. Air jet, Vibrating mesh and Ultrasonic) employing two airflow rates i.e. 60 and 15 L/min. Data are mean \pm SD, n = 3

| Characterization | Air jet | Vibrating mesh | Ultrasonic |
|------------------------|------------------|------------------|------------------|
| 60 L/min | | | |
| FPD (μg) | 90.45 \pm 5.47 | 84.15 \pm 4.36 | 36.53 \pm 3.69 |
| FPF (%) | 69.56 \pm 3.80 | 64.72 \pm 3.24 | 28.12 \pm 2.84 |
| RF (%) | 91.99 \pm 2.29 | 78.27 \pm 3.13 | 88.18 \pm 3.86 |
| MMAD (μm) | 1.15 \pm 0.32 | 4.40 \pm 0.14 | 2.18 \pm 0.11 |
| GSD | 2.32 \pm 0.04 | 2.15 \pm 0.06 | 1.79 \pm 0.04 |
| 15 L/min | | | |
| FPD (μg) | 69.47 \pm 3.43 | 68.44 \pm 3.52 | 18.76 \pm 1.19 |
| FPF (%) | 54.36 \pm 2.56 | 55.72 \pm 2.52 | 14.44 \pm 1.12 |
| RF (%) | 69.43 \pm 3.84 | 63.01 \pm 4.29 | 67.65 \pm 3.18 |
| MMAD (μm) | 1.62 \pm 0.17 | 4.31 \pm 0.13 | 2.06 \pm 0.14 |
| GSD | 2.48 \pm 0.11 | 2.28 \pm 0.06 | 1.79 \pm 0.11 |

Using airflow rates of 60 and 15 L/min, significantly higher RF was observed for the Air jet nebulizer, followed by the Ultrasonic and lastly the Vibrating mesh nebulizer (Table 4). Although demonstrating a similar trend in terms of nebulizer differences, overall RF was observed to be significantly lower ($p < 0.05$) for airflow rate of 15 L/min when compared to 60 L/min. At both 60 and 15 L/min airflow rates, the Air jet and Ultrasonic nebulizer deposited a higher volume of RF in the NGI stages, with droplet size $< 5 \mu\text{m}$ (less than this size are considered as respirable fraction) (O'Callaghan and Barry, 1997). It is noteworthy that for this specific aerodynamic diameter, NGI stages 2 – 7 and 4 – 7 were selected for 60 and 15 L/min, respectively (Table 4) (Section 2.7). Upon aerosolization, it was noted that at a 60 L/min airflow rate, droplets with an aerodynamic diameter $< 5 \mu\text{m}$ were able to travel further into the latter stages of the NGI, this was observed for the majority of the formulation, related to the smaller droplet size. Whereas, droplets above this size demonstrated a tendency to deposit in the initial stages of the NGI (induction port and stage 1) due to inertial impaction. Conversely, when utilising the lower airflow rate (i.e. 15 L/min), the formulations were unable to pass through the initial stages of the NGI (induction port and stages 1, 2 and 3) to achieve desirable deposition in the lower stages. Furthermore, it may also suggested that the higher airflow rate possess higher suction, which further reduce droplet aggregation/fusion and hence improve deposition in the lateral stages of NGI.

3.9. Mass median aerodynamic diameter (MMAD) and geometric standard deviation (GSD) of NLCs F10 formulation

A critical parameter which impacts upon particle deposition in the different stages of NGI and thus in the respiratory tract is MMAD. MMAD is the aerodynamic diameter at which 50% of the aerosolized mass are smaller lies below the stated diameter. Whilst an ideal particle size has not been identified, MMAD typically should be $\leq 5 \mu\text{m}$ in order to reach smaller airways to achieve peripheral deposition. A trend of smaller to larger droplet size for MMAD was observed for the Air jet nebulizer, followed by the Ultrasonic and lastly Vibrating mesh nebulizer (Table 4). No significant difference ($p>0.05$) was noted between MMAD values using two different airflow rates (i.e. 60 and 15 L/min). However, upon analysis of MMAD, it was found that all three nebulizers using both higher and lower airflow rate demonstrated a deposition less than $5 \mu\text{m}$ (Table 4). MMAD less than $5 \mu\text{m}$ is recognized cut-off point for formulation deposition in the alveolar region, indicating that all three nebulizers using BDP-NLCs F10 formulation were highly efficient.

It is also established that the lower the size, the better the deposition in the alveolar region of the pulmonary system. Overall, the Air jet nebulizer was observed to generate MMAD of smaller size than the Vibrating mesh nebulizer. This may be confirmed by the deposition of higher concentration of BDP (using the Air jet nebulizer) in the middle to lateral stages of NGI at both 60 and 15 L/min airflow rate (Figure 3a and b). Contrastingly, the Vibrating mesh nebulizer exhibited higher BDP deposition in the initial stages and lower in the lateral stages at both 60 and 15 airflow rates (Figure 3a and b). Previous researcher also confirmed these results, where jet nebulizer exhibited smaller MMAD when compared to mesh nebulizer (Abdelrahim, 2011, Adorni et al., 2019, Abdou et al., 2019).

GSD values demonstrated no significant difference ($p>0.05$) when two different airflow rates were employed. However, values were significantly higher for the Air jet nebulizer when compared to the Vibrating mesh and followed by the Ultrasonic nebulizer (Table 4). Values using NGI were lower than 2.5 for all three nebulizers at both airflow rates (i.e. 60 and 15 L/min). These results are in agreement with GSD values recorded in research conducted by Adorni et al. (2019) and Zhou et al. (2005).

Conclusions

In this study, versatile BDP-NLC formulations were designed, developed and optimized with inimitable combination of a selected solid lipids and liquid lipids for pulmonary drug delivery.

Moreover, better aerosolization performance was achieved by Air jet nebulizer using NGI at both airflow rates (i.e. 60 and 15 L/min). Various combinations of three liquid lipid and five solid lipids were used to prepare 15 BDP-NLC formulations. Upon initial analysis of stability amongst all BDP-NLC formulations, the F10 formulation (containing PGD as a liquid lipid and GTL as liquid lipid) was selected based on smaller particle size (219 – 225 nm), lower polydispersity index (i.e. 0.22 – 0.24) and higher entrapment efficiency (>90%) using three different temperature conditions (i.e. 4, 25 and 45 °C) for six weeks. A combination of liquid and solid lipid have highlighted the selection and development of BDP-NLC formulations for potential drug delivery using NLCs in the future. Following nebulization performance employing the F10 formulation with both high and low airflow rates (i.e. 60 and 15 L/min), the Air jet nebulizer deposited the highest concentration of BDP in the lateral stages of NGI (>80%), making it suitable nebulizer for targeting lower lungs. Upon comparison to the Vibrating mesh and Ultrasonic nebulizers, the Air jet nebulizer was notably efficient in depositing higher FPD, FPF, RF and lower MMAD of the F10 formulation in the NGI stages at both airflow rates. The Air jet nebulizer was suggested to be significantly better in terms of aerosolization performance overall.

Acknowledgment

We are very thankful to Oleo chemicals, UK for their generous supply of Propylene glycol dicaprylate/dicaprate (Miglyol 840), glycerol trimyristate (Trimyristin).

Funding

This research did not receive any specific grant from funding agencies in the public, commercial, or not for profit sectors.

Declaration of Interest

None.

References

- ABDELRAHIM, M. E. 2011. Aerodynamic characteristics of nebulized terbutaline sulphate using the Andersen Cascade Impactor compared to the Next Generation Impactor. *Pharmaceutical Development and Technology*, 16, 137-145.
- ABDELRAHIM, M. E., PLANT, P. & CHRYSSTYN, H. 2010. In-vitro characterisation of the nebulised dose during non-invasive ventilation. *J Pharm Pharmacol*, 62, 966-72.
- ABDOU, E. M., KANDIL, S. M., MORSI, A. & SLEEM, M. W. 2019. In-vitro and in-vivo respiratory deposition of a developed metered dose inhaler formulation of an anti-migraine drug. *Drug Deliv*, 26, 689-699.
- ADORNI, G., SEIFERT, G., BUTTINI, F., COLOMBO, G., STECANELLA, L. A., KRÄMER, I. & ROSSI, A. 2019. Aerosolization Performance of Jet Nebulizers and Biopharmaceutical Aspects. *Pharmaceutics*, 11, 406.
- BARBOSA, J. P., NEVES, A. R., SILVA, A. M., BARBOSA, M. A., REIS, M. S. & SANTOS, S. G. 2016. Nanostructured lipid carriers loaded with resveratrol modulate human dendritic cells. *Int J Nanomedicine*, 11, 3501-16.
- BECK-BROICHSITTER, M., KLEIMANN, P., SCHMEHL, T., BETZ, T., BAKOWSKY, U., KISSEL, T. & SEEGER, W. 2012. Impact of lyoprotectants for the stabilization of biodegradable nanoparticles on the performance of air-jet, ultrasonic, and vibrating-mesh nebulizers. *European Journal of Pharmaceutics and Biopharmaceutics*, 82, 272-280.
- BNYAN, R., CESARINI, L., KHAN, I., ROBERTS, M. & EHTEZAZI, T. 2020. The effect of ethanol evaporation on the properties of inkjet produced liposomes. *DARU Journal of Pharmaceutical Sciences*, 28, 271-280.
- BNYAN, R., KHAN, I., EHTEZAZI, T., SALEEM, I., GORDON, S., O'NEILL, F. & ROBERTS, M. 2018. Surfactant Effects on Lipid-Based Vesicles Properties. *Journal of Pharmaceutical Sciences*, 107, 1237-1246.
- BNYAN, R., KHAN, I., EHTEZAZI, T., SALEEM, I., GORDON, S., O'NEILL, F. & ROBERTS, M. 2019. Formulation and optimisation of novel transfersomes for sustained release of local anaesthetic. *Journal of Pharmacy and Pharmacology*, 71, 1508-1519.
- CAO, C., WANG, Q. & LIU, Y. 2019. Lung cancer combination therapy: doxorubicin and β -elemene co-loaded, pH-sensitive nanostructured lipid carriers. *Drug design, development and therapy*, 13, 1087-1098.
- COPLEY, M. 2008. Nebulizer testing, Exploring the implications of new regulatory guidance for testing nebulizers. www.inhalationmag.com. 1-4, Access date 5th October 2020, <https://www.inhalationmag.com/?s=Nebulizer+testing&search=>.
- D'ANGELO, I., CONTE, C., MIRO, A., QUAGLIA, F. & UNGARO, F. 2015. Pulmonary drug delivery: a role for polymeric nanoparticles? *Curr Top Med Chem*, 15, 386-400.
- DHAND, R. 2002. Nebulizers that use a vibrating mesh or plate with multiple apertures to generate aerosol. *Respir Care*, 47, 1406-16.
- DHAND, R. 2008. Aerosol Delivery During Mechanical Ventilation: From Basic Techniques to New Devices *Journal of Aerosol Medicine and Pulmonary Drug Delivery*, 21, 45-60.
- EL-SALAMOUNI, N. S., FARID, R. M., EL-KAMEL, A. H. & EL-GAMAL, S. S. 2015. Effect of sterilization on the physical stability of brimonidine-loaded solid lipid nanoparticles and nanostructured lipid carriers. *International Journal of Pharmaceutics*, 496, 976-983.
- ELHISSI, A. 2017. Liposomes for Pulmonary Drug Delivery: The Role of Formulation and Inhalation Device Design. *Curr Pharm Des*, 23, 362-372.
- ELHISSI, A., GILL, H., AHMED, W. & TAYLOR, K. 2011. Vibrating-mesh nebulization of liposomes generated using an ethanol-based proliposome technology. *J Liposome Res*, 21, 173-180.
- ELHISSI, A. & TAYLOR, K. M. G. 2005. Delivery of liposomes generated from pro liposomes using air-jet, ultrasonic and vibrating-mesh nebulisers. *J. Drug Del. Sci. Technol.*, 15, 261-265.
- ELHISSI, A. M. A., FAIZI, M., NAJI, W. F., GILL, H. S. & TAYLOR, K. M. G. 2007. Physical stability and aerosol properties of liposomes delivered using an air-jet nebulizer and a novel micropump device with large mesh apertures. *International Journal of Pharmaceutics*, 334, 62-70.

- ESMAEILI, M., AGHAJANI, M., ABBASALIPOURKABIR, R. & AMANI, A. 2016. Budesonide-loaded solid lipid nanoparticles for pulmonary delivery: preparation, optimization, and aerodynamic behavior. *Artif Cells Nanomed Biotechnol*, 44, 1964-1971.
- GALA, R. P., KHAN, I., ELHISSI, A. M. & ALHNAN, M. A. 2015. A comprehensive production method of self-cryoprotected nano-liposome powders. *Int J Pharm*, 486, 153-8.
- HAIDER, M., ABDIN, S. M., KAMAL, L. & ORIVE, G. 2020. Nanostructured Lipid Carriers for Delivery of Chemotherapeutics: A Review. *Pharmaceutics*, 12, 288.
- HEINEMANN, L., PFUTZNER, A. & HEISE, T. 2001. Alternative routes of administration as an approach to improve insulin therapy: update on dermal, oral, nasal and pulmonary insulin delivery. *Curr Pharm Des*, 7, 1327-51.
- HESS, D., FISHER, D., WILLIAMS, P., POOLER, S. & KACMAREK, R. M. 1996. Medication nebulizer performance. Effects of diluent volume, nebulizer flow, and nebulizer brand. *Chest*, 110, 498-505.
- HU, F.-Q., JIANG, S.-P., DU, Y.-Z., YUAN, H., YE, Y.-Q. & ZENG, S. 2006. Preparation and characteristics of monostearin nanostructured lipid carriers. *International Journal of Pharmaceutics*, 314, 83-89.
- ISMAIL, N. E. & CHRYSTYN, H. 2004. The relative bioavailability of salbutamol to the lungs from a U22 MicroAir Nebuliser. *Journal of Pharmacy and Pharmacology*, 56, 43-51.
- JARAI, B. M., KOLEWE, E. L., STILLMAN, Z. S., RAMAN, N. & FROMEN, C. A. 2020. Chapter 18 - Polymeric Nanoparticles. In: CHUNG, E. J., LEON, L. & RINALDI, C. (eds.) *Nanoparticles for Biomedical Applications*. Elsevier.
- KELIDARI, H. R., SAEEDI, M., AKBARI, J., MORTEZA-SEMNANI, K., VALIZADEH, H., MANIRUZZAMAN, M., FARMOUDEH, A. & NOKHODCHI, A. 2017. Development and Optimisation of Spironolactone Nanoparticles for Enhanced Dissolution Rates and Stability. *AAPS PharmSciTech*, 18, 1469-1474.
- KHAN, I., APOSTOLOU, M., BNYAN, R., HOUACINE, C., ELHISSI, A. & YOUSAF, S. S. 2020a. Paclitaxel-loaded micro or nano transfersome formulation into novel tablets for pulmonary drug delivery via nebulization. *Int J Pharm*, 575, 118919.
- KHAN, I., ELHISSI, A., SHAH, M., ALHNAN, M. A. & WAQAR, A. 2013. Liposome-based carrier systems and devices used for pulmonary drug delivery. In: DAVIM, J. P. (ed.) *Biomaterial and medical tribology research and development*. Cambridge, UK: Woodhead Publishing Limited,.
- KHAN, I., YOUSAF, S., ALHNAN, M. A., AHMED, W., ELHISSI, A. & JACKSON, M. J. 2016. Design Characteristics of Inhaler Devices Used for Pulmonary Delivery of Medical Aerosols. In: AHMED, W. & JACKSON, M. J. (eds.) *Surgical Tools and Medical Devices*. Cham: Springer International Publishing, pp: 573-591.
- KHAN, I., YOUSAF, S., NAJLAH, M., AHMED, W. & ELHISSI, A. 2020c. Proliposome powder or tablets for generating inhalable liposomes using a medical nebulizer. *Journal of Pharmaceutical Investigation*.
- KHAN, I., YOUSAF, S., SUBRAMANIAN, S., ALHNAN, M. A., AHMED, W. & ELHISSI, A. 2018. Proliposome Powders for the Generation of Liposomes: the Influence of Carbohydrate Carrier and Separation Conditions on Crystallinity and Entrapment of a Model Antiasthma Steroid. *AAPS PharmSciTech*, 19, 262-274.
- KUMAR, R., YASIR, M., SARAF, S. A., GAUR, P. K., KUMAR, Y. & SINGH, A. P. 2013. Glyceryl monostearate based nanoparticles of mefenamic acid: Fabrication and in vitro characterization. *Drug Invention Today*, 5, 246-250.
- LIU, J., GONG, T., FU, H., WANG, C., WANG, X., CHEN, Q., ZHANG, Q., HE, Q. & ZHANG, Z. 2008. Solid lipid nanoparticles for pulmonary delivery of insulin. *International Journal of Pharmaceutics*, 356, 333-344.
- MAHANT, S., RAO, R. & NANDA, S. 2018. Chapter 3 - Nanostructured lipid carriers: Revolutionizing skin care and topical therapeutics. In: GRUMEZESCU, A. M. (ed.) *Design of Nanostructures for Versatile Therapeutic Applications*. William Andrew Publishing.

- MAKONI, P. A., WA KASONGO, K. & WALKER, R. B. 2019. Short Term Stability Testing of Efavirenz-Loaded Solid Lipid Nanoparticle (SLN) and Nanostructured Lipid Carrier (NLC) Dispersions. *Pharmaceutics*, 11, 397.
- MALAMATARI, M., CHARISI, A., MALAMATARIS, S., KACHRIMANIS, K. & NIKOLAKAKIS, I. 2020. Spray Drying for the Preparation of Nanoparticle-Based Drug Formulations as Dry Powders for Inhalation. *Processes*, 8, 788.
- MARPLE, V. A., OLSON, B. A., SANTHANAKRISHNAN, K., MITCHELL, J. P., MURRAY, S. C. & HUDSON-CURTIS, B. L. 2003. Next generation pharmaceutical impactor (a new impactor for pharmaceutical inhaler testing). Part II: Archival calibration. *J Aerosol Med*, 16, 301-24.
- MARPLE, V. A., OLSON, B. A., SANTHANAKRISHNAN, K., ROBERTS, D. L., MITCHELL, J. P. & HUDSON-CURTIS, B. L. 2004. Next generation pharmaceutical impactor: a new impactor for pharmaceutical inhaler testing. Part III. extension of archival calibration to 15 L/min. *J Aerosol Med*, 17, 335-43.
- MEHNERT, W. & MÄDER, K. 2001. Solid lipid nanoparticles: Production, characterization and applications. *Advanced Drug Delivery Reviews*, 47, 165-196.
- MORIN, C. M. D., IVEY, J. W., TITOSKY, J. T. F., SUDERMAN, J. D., OLFERT, J. S., VEHRING, R. & FINLAY, W. H. 2014. Performance of pressurized metered-dose inhalers at extreme temperature conditions. *J Pharm Sci*, 103, 3553-3559.
- MUZZALUPO, R. & MAZZOTTA, E. 2019. Do niosomes have a place in the field of drug delivery? *Expert Opinion on Drug Delivery*, 16, 1145-1147.
- NAFEE, N., MAKLED, S. & BORAIE, N. 2018. Nanostructured lipid carriers versus solid lipid nanoparticles for the potential treatment of pulmonary hypertension via nebulization. *Eur J Pharm Sci*, 125, 151-162.
- NAJLAH, M., HIDAYAT, K., OMER, H. K., MWESIGWA, E., AHMED, W., ALOBAIDY, K. G., PHOENIX, D. A. & ELHISSI, A. 2015. A facile approach to manufacturing non-ionic surfactant nanodispersions using proniosome technology and high-pressure homogenization. *Journal of Liposome Research*, 25, 32-37.
- NASRI, S., EBRAHIMI-HOSSEINZADEH, B., RAHAIE, M., HATAMIAN-ZARMI, A. & SAHRAEIAN, R. 2020. Thymoquinone-loaded ethosome with breast cancer potential: optimization, in vitro and biological assessment. *Journal of Nanostructure in Chemistry*, 10, 19-31.
- NESAMONY, J., SHAH, I. S., KALRA, A. & JUNG, R. 2014. Nebulized oil-in-water nanoemulsion mists for pulmonary delivery: development, physico-chemical characterization and in vitro evaluation. *Drug Development and Industrial Pharmacy*, 40, 1253-1263.
- O'CALLAGHAN, C. & BARRY, P. W. 1997. The science of nebulised drug delivery. *Thorax*, 52 Suppl 2, S31-44.
- OLBRICH, C., KAYSER, O. & MÜLLER, R. H. 2002. Lipase degradation of Dynasan 114 and 116 solid lipid nanoparticles (SLN)—effect of surfactants, storage time and crystallinity. *International Journal of Pharmaceutics*, 237, 119-128.
- PAVONI, L., PERINELLI, D. R., BONACUCINA, G., CESPI, M. & PALMIERI, G. F. 2020. An Overview of Micro- and Nanoemulsions as Vehicles for Essential Oils: Formulation, Preparation and Stability. *Nanomaterials (Basel)*, 10, 135.
- PHIPPS, P. R. & GONDA, I. 1990. Droplets produced by medical nebulizers. some factors affecting their size and solute concentration. *CHEST Journal*, 97, 1327-1332.
- PINDIPROLU, S. K. S. S., KUMAR, C. S. P., KUMAR GOLLA, V. S., P, L., K, S. C., S K, E. B. & R K, R. 2020. Pulmonary delivery of nanostructured lipid carriers for effective repurposing of salinomycin as an antiviral agent. *Medical hypotheses*, 143, 109858.
- RAU, J. L. 2002. Design principles of liquid nebulization devices currently in use. *Respir Care*, 47, 1257-75; discussion 1275-8.
- SAHITO, B., ZHANG, Q., YANG, H., PENG, L., GAO, X., KASHIF, J., UL AABDIN, Z., JIANG, S., WANG, L. & GUO, D. 2020. Synthesis of Tilmicosin Nanostructured Lipid Carriers for Improved Oral

- Delivery in Broilers: Physicochemical Characterization and Cellular Permeation. *Molecules*, 25, 315.
- SAUPE, A., WISSING, S. A., LENK, A., SCHMIDT, C. & MULLER, R. H. 2005. Solid lipid nanoparticles (SLN) and nanostructured lipid carriers (NLC) -- structural investigations on two different carrier systems. *Biomed Mater Eng*, 15, 393-402.
- SHAFIQUE, M., KHAN, M. A., KHAN, W. S., MAQSOOD UR, R., AHMAD, W. & KHAN, S. 2017. Fabrication, Characterization, and In Vivo Evaluation of Famotidine Loaded Solid Lipid Nanoparticles for Boosting Oral Bioavailability. *Journal of Nanomaterials*, 2017, 1-10.
- SHAH, N. V., SETH, A. K., BALARAMAN, R., AUNDHIA, C. J., MAHESHWARI, R. A. & PARMAR, G. R. 2016. Nanostructured lipid carriers for oral bioavailability enhancement of raloxifene: Design and in vivo study. *Journal of advanced research*, 7, 423-434.
- SUBRAMANIAM, B., SIDDIK, Z. H. & NAGOOR, N. H. 2020. Optimization of nanostructured lipid carriers: understanding the types, designs, and parameters in the process of formulations. *Journal of Nanoparticle Research*, 22, 141.
- SUBRAMANIAN, S., KHAN, I., KORALE, O., ALHNAN, M. A., AHMED, W., NAJLAH, M., TAYLOR, K. M. G. & ELHISSI, A. 2016. A simple approach to predict the stability of phospholipid vesicles to nebulization without performing aerosolization studies. *International Journal of Pharmaceutics*, 502, 18-27.
- SWEENEY, L., MCCLOSKEY, A. P., HIGGINS, G., RAMSEY, J. M., CRYAN, S.-A. & MACLOUGHLIN, R. 2019. Effective nebulization of interferon- γ using a novel vibrating mesh. *Respiratory Research*, 20, 66.
- THATIPAMULA, R., PALEM, C., GANNU, R., MUDRAGADA, S. & YAMSANI, M. 2011. Formulation and in vitro characterization of domperidone loaded solid lipid nanoparticles and nanostructured lipid carriers. *Daru : journal of Faculty of Pharmacy, Tehran University of Medical Sciences*, 19, 23-32.
- UNG, K. T., RAO, N., WEERS, J. G., CLARK, A. R. & CHAN, H.-K. 2014. In Vitro Assessment of Dose Delivery Performance of Dry Powders for Inhalation. *Aerosol Science and Technology*, 48, 1099-1110.
- WEBER, S., ZIMMER, A. & PARDEIKE, J. 2014. Solid Lipid Nanoparticles (SLN) and Nanostructured Lipid Carriers (NLC) for pulmonary application: A review of the state of the art. *European Journal of Pharmaceutics and Biopharmaceutics*, 86, 7-22.
- ZHANG, X., LIU, Q., HU, J., XU, L. & TAN, W. 2014. An aerosol formulation of R-salbutamol sulfate for pulmonary inhalation. *Acta Pharm Sin B*, 4, 79-85.
- ZHOU, Y., AHUJA, A., IRVIN, C. M., KRACKO, D. A., MCDONALD, J. D. & CHENG, Y. S. 2005. Medical nebulizer performance: effects of cascade impactor temperature. *Respir Care*, 50, 1077-82.

CRedit authorship contribution statement

Iftikhar Khan: Conceptualization, Supervision, Writing - Original draft preparation. **Sozan Hussein:** Data curation, Methodology. **Chahinez Houacine:** Resources, Data curation. **Sajid K. Sadozai:** Visualization. **Ruba Bnyan:** Software. **Ruba Bnyan:** Validation. **Abdelbary Elhissi:** Editing. **Sakib S. Yousaf:** Investigation, Writing - Review & Editing.

Journal Pre-proofs

Figure 1

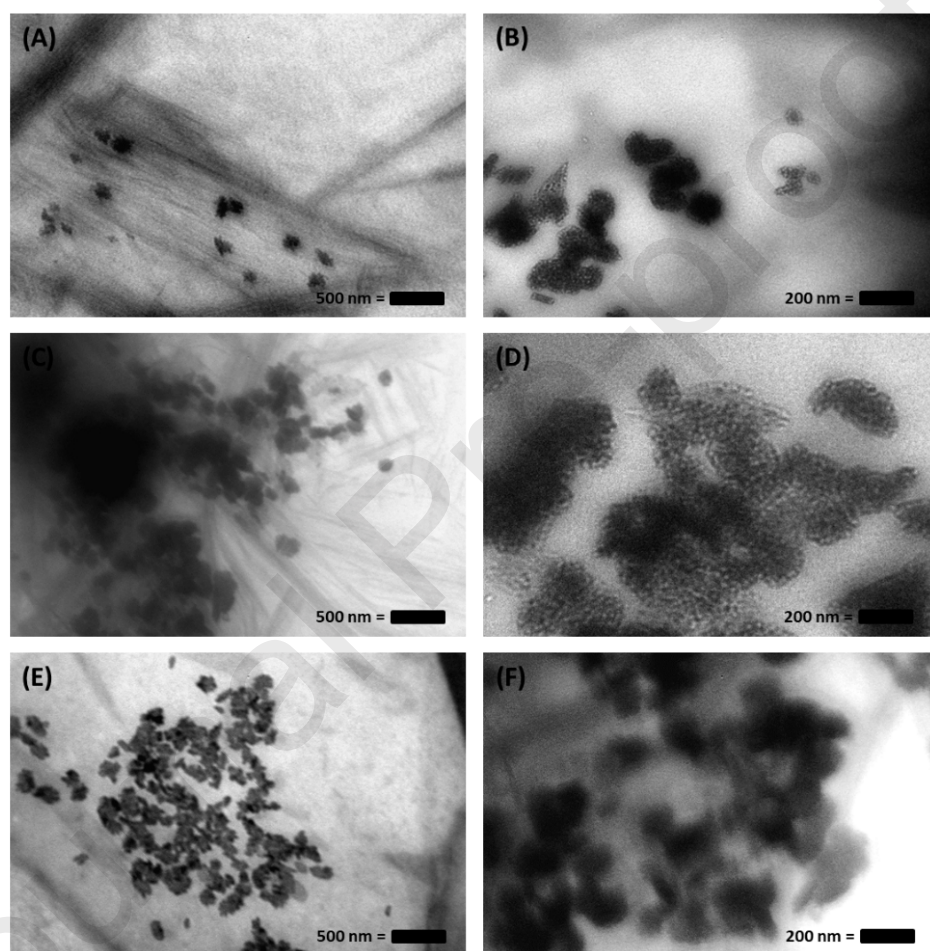


Figure 1: TEM images of BDP-NLCs (A and B) F7, (C and D) F8 and, (E and F) F10 formulations with two different magnifications. These images are typical of three such different experiments

Figure 2

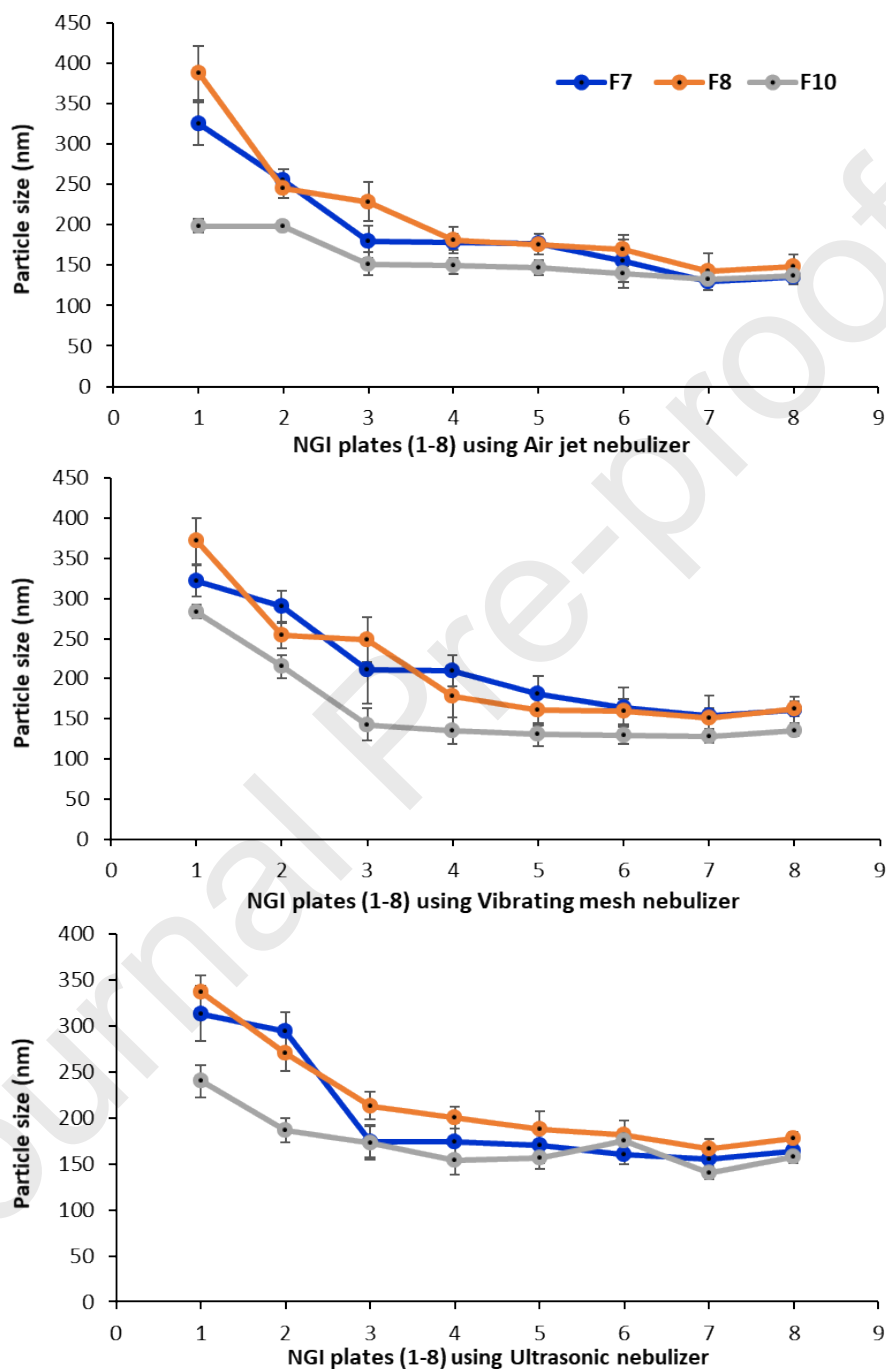


Figure 2: Deposition of aerosol droplets containing BDP-NLCs particles in various stages of NGI (i.e. 1 – 8) using formulations F7, F8 and F10 after aerosolization using 60 L/min employing an Air jet, Vibrating mesh and Ultrasonic nebulizers. Data are mean \pm SD, n = 3

Figure 3

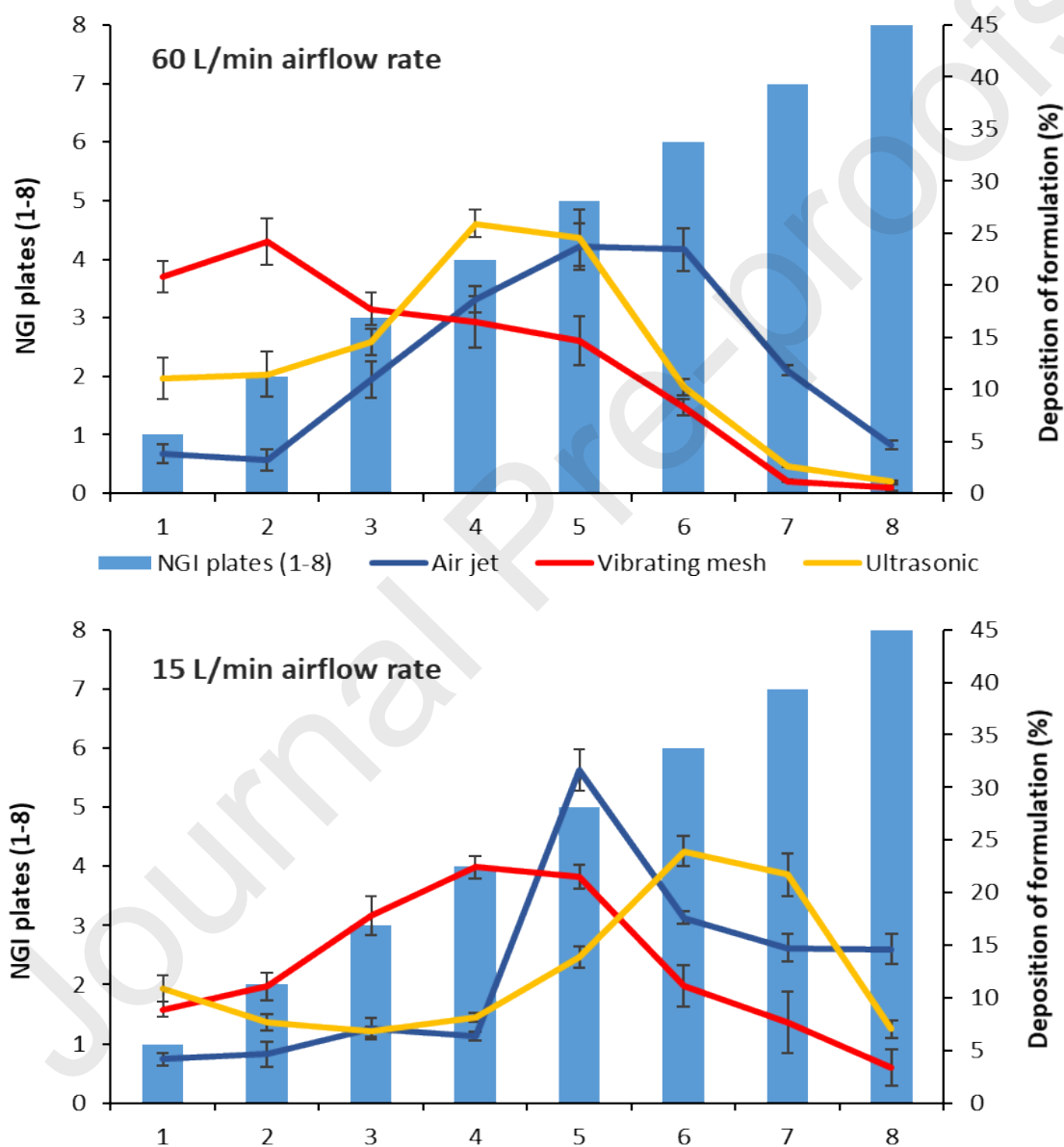


Figure 3: Deposition of BDP of NLCs F10 formulation in various stages (1 – 8) of the NGI (with the cut-off diameter of each stage) employing three nebulizers (i.e. Air jet, Vibrating mesh and Ultrasonic) for aerosolization using two different airflow rates i.e. 60 and 15 L/min. Data are mean \pm SD, n = 3

Figure 4

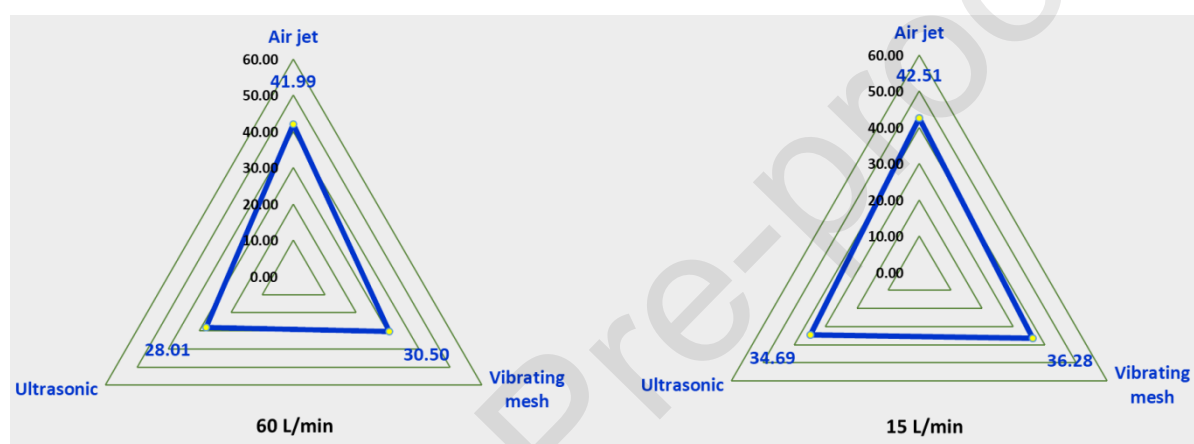


Figure 4: Nebulization time of BDP-NLCs F10 formulations using three nebulizers (i.e. Air jet, Vibrating mesh and Ultrasonic) employing two airflow rates i.e. 60 and 15 L/min. Data are mean \pm SD, n = 3

Figure 5

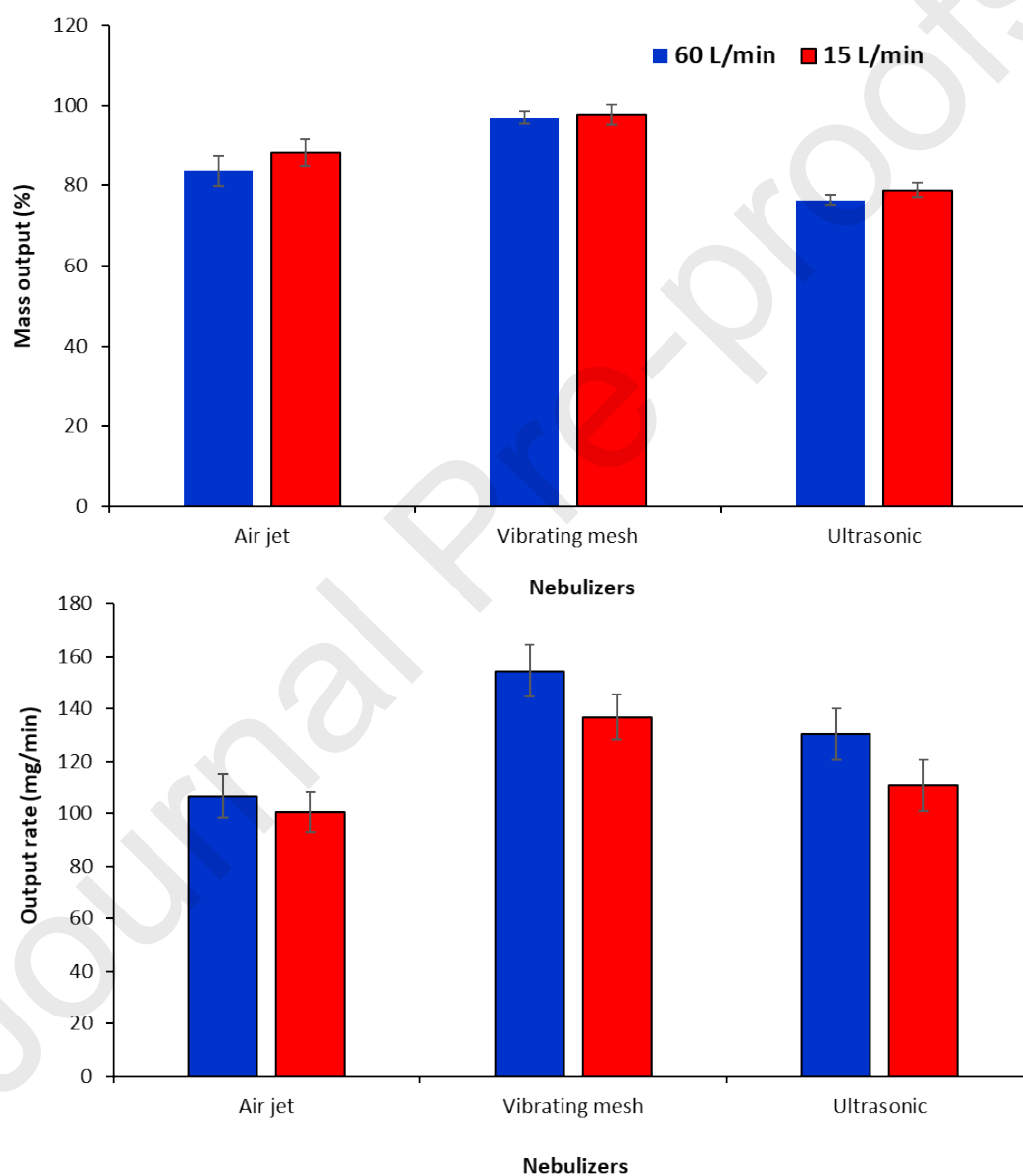


Figure 5: Mass output and output rate of BDP-NLCs F10 formulations after aerosolization using three nebulizers (i.e. Air jet, Vibrating mesh and Ultrasonic) employing two different airflow rates i.e. 60 and 15 L/min. Data are mean \pm SD, n = 3

Table 1

Table 1. Composition of NLCs formulations using three liquid lipids (isopropyl palmitate (IPP), propylene glycol dicaprylate/dicaprate (PGD) and glyceryl tributyrate (GTB)) and five solid lipids (glycerol trimyristate (GTM), stearic acid (SA), glycerol monostearate (GMS), cetyl palmitate (CP) and glycerol trilaurate (GTL)) of lipid phase were used in 3:1 w/w ratios with a model drug Beclomethasone dipropionate (BDP) (2.6 mg) in order to manufacture fifteen BDP-NLCs formulations. Data are mean \pm SD, n = 3

| Formulations | Liquid Lipid | Solid Lipid |
|---------------------|--|-------------------------------|
| F1 | Isopropyl palmitate | Glycerol trimyristate |
| F2 | Isopropyl palmitate | Stearic acid |
| F3 | Isopropyl palmitate | Glycerol monostearate |
| F4 | Isopropyl palmitate | Cetyl palmitate |
| F5 | Isopropyl palmitate | Glyceryl trilaurate |
| F6 | Propylene glycol dicaprylate/dicaprate | Glycerol trimyristate |
| F7 | Propylene glycol dicaprylate/dicaprate | Stearic acid |
| F8 | Propylene glycol dicaprylate/dicaprate | Glycerol monostearate |
| F9 | Propylene glycol dicaprylate/dicaprate | Cetyl palmitate |
| F10 | Propylene glycol dicaprylate/dicaprate | Glyceryl trilaurate |
| F11 | Glyceryl tributyrate | Glycerol trimyristate |
| F12 | Glyceryl tributyrate | Stearic acid |
| F13 | Glyceryl tributyrate | Glycerol monostearate |
| F14 | Glyceryl tributyrate | Cetyl palmitate |
| F15 | Glyceryl tributyrate | Glyceryl trilaurate Trilaurin |

Table 2

Table 2: Particle size, polydispersity index (PDI), Zeta potential and entrapment efficiency of Beclomethasone dipropionate (BDP) of freshly prepared BDP-NLCs formulations (F1 – F15), as well as after one week of stability at 25 °C. Data are mean \pm SD, n = 3

| Formulations | Size (nm) | | PDI | | Zeta potential (mV) | | Entrapment efficiency (%) | |
|--------------|-------------------|--------------------|-------------------|--------------------|---------------------|--------------------|---------------------------|--------------------|
| | After preparation | 25 °C after 1 week | After preparation | 25 °C after 1 week | After preparation | 25 °C after 1 week | After preparation | 25 °C after 1 week |
| F1 | 226.31 \pm 5.57 | 285.52 \pm 6.34 | 0.29 \pm 0.01 | 0.45 \pm 0.02 | -4.31 \pm 1.02 | -4.66 \pm 1.36 | 94.26 \pm 4.32 | 92.51 \pm 4.76 |
| F2 | 201.54 \pm 6.21 | 255.31 \pm 5.71 | 0.26 \pm 0.01 | 0.59 \pm 0.03 | -8.26 \pm 1.54 | -9.74 \pm 2.03 | 93.73 \pm 5.24 | 91.75 \pm 5.61 |
| F3 | 436.30 \pm 4.33 | 477.26 \pm 4.68 | 0.45 \pm 0.03 | 0.75 \pm 0.05 | -7.36 \pm 1.28 | -9.67 \pm 2.51 | 94.33 \pm 6.42 | 91.79 \pm 4.91 |
| F4 | 245.18 \pm 6.25 | 269.85 \pm 5.27 | 0.41 \pm 0.03 | 0.58 \pm 0.03 | -13.64 \pm 2.81 | -15.72 \pm 3.17 | 94.07 \pm 5.16 | 93.57 \pm 4.83 |
| F5 | 244.19 \pm 7.26 | 493.88 \pm 7.61 | 0.34 \pm 0.03 | 0.77 \pm 0.06 | -6.39 \pm 1.82 | -8.06 \pm 2.61 | 90.08 \pm 5.77 | 89.74 \pm 5.37 |
| F6 | 253.18 \pm 5.16 | 268.15 \pm 5.06 | 0.43 \pm 0.03 | 0.58 \pm 0.02 | -6.79 \pm 1.34 | -5.18 \pm 1.06 | 93.52 \pm 6.05 | 90.73 \pm 5.71 |
| F7 | 241.20 \pm 5.73 | 239.55 \pm 5.06 | 0.24 \pm 0.03 | 0.24 \pm 0.02 | -4.27 \pm 1.02 | -3.55 \pm 1.06 | 96.88 \pm 4.76 | 94.37 \pm 4.06 |
| F8 | 233.41 \pm 4.38 | 228.97 \pm 5.53 | 0.26 \pm 0.02 | 0.23 \pm 0.02 | -3.54 \pm 0.98 | -3.44 \pm 0.87 | 95.64 \pm 4.39 | 91.38 \pm 5.03 |
| F9 | 244.35 \pm 6.05 | 283.58 \pm 8.01 | 0.36 \pm 0.01 | 0.52 \pm 0.04 | -4.92 \pm 1.17 | -3.65 \pm 1.12 | 94.46 \pm 5.28 | 92.46 \pm 5.61 |
| F10 | 223.69 \pm 5.51 | 217.87 \pm 6.34 | 0.26 \pm 0.02 | 0.25 \pm 0.02 | -1.36 \pm 0.06 | -1.24 \pm 0.07 | 94.56 \pm 6.44 | 91.92 \pm 5.39 |
| F11 | 245.24 \pm 8.15 | 313.63 \pm 7.74 | 0.36 \pm 0.01 | 0.63 \pm 0.04 | -8.81 \pm 2.37 | -8.23 \pm 1.86 | 92.68 \pm 6.62 | 88.97 \pm 5.44 |
| F12 | 262.65 \pm 7.25 | 308.53 \pm 6.81 | 0.26 \pm 0.03 | 0.64 \pm 0.03 | -12.64 \pm 3.16 | -10.83 \pm 2.76 | 93.54 \pm 5.70 | 90.17 \pm 4.71 |
| F13 | 270.45 \pm 5.67 | 294.21 \pm 6.62 | 0.31 \pm 0.02 | 0.58 \pm 0.02 | -14.59 \pm 4.35 | -11.84 \pm 3.43 | 90.16 \pm 4.94 | 87.26 \pm 5.87 |
| F14 | 257.91 \pm 5.59 | 324.26 \pm 7.18 | 0.34 \pm 0.03 | 0.61 \pm 0.04 | -12.66 \pm 3.71 | -12.55 \pm 3.65 | 93.34 \pm 5.48 | 90.59 \pm 6.31 |
| F15 | 339.64 \pm 5.64 | 379.23 \pm 6.26 | 0.53 \pm 0.03 | 0.73 \pm 0.05 | -5.49 \pm 1.31 | -7.64 \pm 1.66 | 90.09 \pm 5.51 | 93.46 \pm 5.94 |

Table 3

Table 3: Particle size and particle size distribution (i.e. PDI) of BDP-NLCs F7, F8 and F10 formulations after two, four and six week of stability studies using three different temperature conditions (i.e. 4, 25 and 45 °C). Data are mean \pm SD, n = 3

| Formulations | F7 | | F8 | | F10 | |
|---------------|-------------------|-----------------|-------------------|-----------------|-------------------|-----------------|
| | Size (nm) | PDI | Size (nm) | PDI | Size (nm) | PDI |
| Week 2 | | | | | | |
| 4 °C | 676.45 \pm 8.54 | 0.85 \pm 0.13 | 408.41 \pm 6.15 | 0.65 \pm 0.09 | 220.65 \pm 5.86 | 0.22 \pm 0.06 |
| 25 °C | 247.63 \pm 5.94 | 0.36 \pm 0.09 | 234.81 \pm 4.64 | 0.29 \pm 0.07 | 219.43 \pm 6.28 | 0.24 \pm 0.08 |
| 45 °C | 245.65 \pm 4.67 | 0.28 \pm 0.06 | 231.59 \pm 5.73 | 0.29 \pm 0.08 | 225.76 \pm 7.07 | 0.23 \pm 0.09 |
| Week 4 | | | | | | |
| 4 °C | 737.81 \pm 9.79 | 0.97 \pm 0.18 | 423.67 \pm 6.63 | 0.68 \pm 0.11 | 227.28 \pm 6.35 | 0.21 \pm 0.05 |
| 25 °C | 251.79 \pm 6.56 | 0.39 \pm 0.11 | 246.54 \pm 6.63 | 0.31 \pm 0.09 | 217.74 \pm 7.15 | 0.25 \pm 0.09 |
| 45 °C | 246.1 \pm 6.72 | 0.27 \pm 0.08 | 233.82 \pm 4.08 | 0.31 \pm 0.10 | 218.27 \pm 6.58 | 0.27 \pm 0.11 |
| Week 6 | | | | | | |
| 4 °C | 727.97 \pm 9.16 | 0.99 \pm 1.15 | 439.83 \pm 7.28 | 0.67 \pm 0.13 | 232.42 \pm 6.61 | 0.22 \pm 0.07 |
| 25 °C | 278.58 \pm 7.25 | 0.43 \pm 0.11 | 265.22 \pm 5.83 | 0.37 \pm 0.08 | 226.49 \pm 7.86 | 0.27 \pm 0.08 |
| 45 °C | 248.18 \pm 5.91 | 0.29 \pm 0.06 | 236.72 \pm 5.37 | 0.35 \pm 0.12 | 221.98 \pm 7.13 | 0.26 \pm 0.08 |

Table 4

Table 4: Aerosol dispersion performance parameters including; fine particle dose (FPD), fine particle fraction (FPF), respirable fraction (RF), mass median aerodynamic diameter (MMAD) and geometric standard deviation (GSD) of BDP-NLCs F10 formulation using three nebulizers (i.e. Air jet, Vibrating mesh and Ultrasonic) employing two airflow rates i.e. 60 and 15 L/min. Data are mean \pm SD, n = 3

| Characterization | Air jet | Vibrating mesh | Ultrasonic |
|------------------------|------------------|------------------|------------------|
| 60 L/min | | | |
| FPD (μg) | 90.45 \pm 5.47 | 84.15 \pm 4.36 | 36.53 \pm 3.69 |
| FPF (%) | 69.56 \pm 3.80 | 64.72 \pm 3.24 | 28.12 \pm 2.84 |
| RF (%) | 91.99 \pm 2.29 | 78.27 \pm 3.13 | 88.18 \pm 3.86 |
| MMAD (μm) | 1.15 \pm 0.32 | 4.40 \pm 0.14 | 2.18 \pm 0.11 |
| GSD | 2.32 \pm 0.04 | 2.15 \pm 0.06 | 1.79 \pm 0.04 |
| 15 L/min | | | |
| FPD (μg) | 69.47 \pm 3.43 | 68.44 \pm 3.52 | 18.76 \pm 1.19 |
| FPF (%) | 54.36 \pm 2.56 | 55.72 \pm 2.52 | 14.44 \pm 1.12 |
| RF (%) | 69.43 \pm 3.84 | 63.01 \pm 4.29 | 67.65 \pm 3.18 |
| MMAD (μm) | 1.62 \pm 0.17 | 4.31 \pm 0.13 | 2.06 \pm 0.14 |
| GSD | 2.48 \pm 0.11 | 2.28 \pm 0.06 | 1.79 \pm 0.11 |

